

In vivo partial reprogramming alters age-associated molecular changes during physiological aging in mice

Kristen C. Browder^{1,11}, Pradeep Reddy^{ID 2,11}, Mako Yamamoto², Amin Haghani^{ID 3,4}, Isabel Guillen Guillen², Sanjeeb Sahu^{ID 2,4}, Chao Wang^{2,4}, Yosu Luque², Javier Prieto², Lei Shi², Kensaku Shojima^{ID 2}, Tomoaki Hishida², Zijuan Lai⁵, Qingling Li⁶, Feroza K. Choudhury⁵, Weng R. Wong⁶, Yuxin Liang⁶, Dewakar Sangaraju⁵, Wendy Sandoval⁶, Concepcion Rodriguez Esteban², Estrella Nuñez Delicado⁷, Pedro Guillen Garcia⁸, Michal Pawlak^{ID 9}, Jason A. Vander Heiden^{ID 9}, Steve Horvath^{ID 3,4,10}, Heinrich Jasper^{ID 1}✉ and Juan Carlos Izpisua Belmonte^{ID 2,4,11}✉

Partial reprogramming by expression of reprogramming factors (Oct4, Sox2, Klf4 and c-Myc) for short periods of time restores a youthful epigenetic signature to aging cells and extends the life span of a premature aging mouse model. However, the effects of longer-term partial reprogramming in physiologically aging wild-type mice are unknown. Here, we performed various long-term partial reprogramming regimens, including different onset timings, during physiological aging. Long-term partial reprogramming lead to rejuvenating effects in different tissues, such as the kidney and skin, and at the organismal level; duration of the treatment determined the extent of the beneficial effects. The rejuvenating effects were associated with a reversion of the epigenetic clock and metabolic and transcriptomic changes, including reduced expression of genes involved in the inflammation, senescence and stress response pathways. Overall, our observations indicate that partial reprogramming protocols can be designed to be safe and effective in preventing age-related physiological changes. We further conclude that longer-term partial reprogramming regimens are more effective in delaying aging phenotypes than short-term reprogramming.

Aging is associated with widespread changes in cells and tissues that can result in chronic inflammation and a decline in metabolic homeostasis^{1–3}. A range of intervention strategies have been identified that can counteract such changes, reduce inflammation, restore metabolic homeostasis and thus delay the onset of age-related diseases^{4–7}. In recent years, cellular reprogramming using transcription factors has emerged as a powerful alternative strategy to rejuvenate aging cells, restore epigenetic marks and erase markers of cell damage, thus reversing cellular phenotypes associated with aging⁸. Ex vivo cellular reprogramming using Oct4, Sox2, Klf4 and c-Myc (OSKM) can completely erase epigenetic states imposed during development, allowing for the conversion of terminally differentiated somatic cells into pluripotent stem cells⁹. This conversion includes erasing aging phenotypes, as demonstrated in reprogrammed cells from individuals of advanced age and patients with premature aging syndromes, such as Hutchinson–Gilford progeria syndrome (HGPS)^{10–12}. Contrary to these beneficial in vitro effects, in vivo expression of reprogramming factors led to the generation of teratomas and death in mice^{13,14}. Following these results, our group was able to demonstrate that in vitro expression of the OSKM factors for short and repeated intervals (thus avoiding

continuous expression) lead to the amelioration of aging hallmarks in fibroblasts obtained from premature aging and normal mice¹⁵ and in human cells from individuals of advanced age in vitro¹⁶. In vivo, partial reprogramming not only prevented the loss of cell identity and the appearance of tumors but also led to an extended life span in an accelerated aging mouse model¹⁵. Subsequently, other groups have shown in different animal models that partial reprogramming reduces fibrosis and scar formation in the skin, ameliorates aging phenotypes in dentate gyrus cells and promotes axon regeneration after injury^{17–19}. We have further found that short-term expression of Yamanaka factors (OSKM) in myofibers can induce satellite cell proliferation and accelerate regeneration in the muscle of young mice²⁰.

Although these are important steps forward to the possibility of using this strategy to increase health and life span in vertebrates, our initial experiments were mainly performed in a mutant background displaying an accelerated aging syndrome. Thus, confounding effects of the mutation (a point mutation in the LMNA gene) on the OSKM-elicited phenotypes could not be ruled out. To allay such concerns and evaluate the feasibility of age reversion by partial OSKM reprogramming more generally, we set out to evaluate the

¹Immunology Discovery, Genentech, Inc., South San Francisco, CA, USA. ²Gene Expression Laboratory, Salk Institute for Biological Studies, La Jolla, CA, USA. ³Department of Human Genetics, David Geffen School of Medicine, University of California Los Angeles, Los Angeles, CA, USA. ⁴Altos Labs, San Diego, CA, USA. ⁵Drug Metabolism and Pharmacokinetics, Genentech, Inc., South San Francisco, CA, USA. ⁶Microchemistry, Proteomics, Lipidomics & Next Generation Sequencing, Genentech, Inc., South San Francisco, CA, USA. ⁷Universidad Católica San Antonio de Murcia, Campus de los Jerónimos, Murcia, Spain. ⁸Clinica CEMTRO, Madrid, Spain. ⁹Bioinformatics, Genentech, Inc., South San Francisco, CA, USA. ¹⁰Department of Biostatistics, University of California Los Angeles, School of Public Health, Los Angeles, CA, USA. ¹¹These authors contributed equally: Kristen C. Browder, Pradeep Reddy.
✉e-mail: jasperh@gene.com; jcbelmonte@altoslabs.com

systemic effects of partial reprogramming in physiologically aging wild-type (WT) mice.

In this study, we report on our observations with regard to two different partial reprogramming long-term treatment regimens (7 and 10 months starting at 15 and 12 months of age, respectively) and a late-onset short-term treatment (1 month started at 25 months of age). In these cohorts, we analyzed the molecular effects of partial reprogramming in different tissues, assessing epigenetic and transcriptomic changes. We further performed untargeted metabolomics and lipidomics of serum samples from animals treated with the 10-month regimen during and at the end of the treatment. Our results show that long-term partial reprogramming is safe and does not lead to obvious negative consequences, such as teratoma formation. Using a methylation clock analysis, we found that in mice that have undergone long-term partial reprogramming, tissues such as the kidney and skin showed a significantly lower biological age. This epigenetic difference is reflected in transcriptomic changes that encompass a reduction in senescence and inflammation signatures. Short-term partial reprogramming, on the other hand, resulted only in minor epigenetic changes and a transcriptional response that was different from the changes elicited by long-term treatment. Long-term partial reprogramming further reduced age-related changes in the metabolite profile of serum, and results in histological changes in the skin, increasing epidermal proliferation and thickness, as well as improving wound healing in old mice. Our results demonstrate that long-term partial reprogramming is a safe and effective strategy to reduce age-related physiological changes.

Results

Long-term *in vivo* partial reprogramming in WT mice is safe. We previously established an *in vivo* partial reprogramming protocol for systemic expression of OSKM by administering doxycycline in drinking water for 2 d followed by 5 d of withdrawal¹⁵ (Fig. 1a). This protocol was sufficient to reduce aging phenotypes and extend life span in a progeria model¹⁵. To test the effects of partial reprogramming in normal aging WT mice, we used mice carrying a single copy of an OSKM polycistronic cassette and a reverse tetracycline transactivator (rtTA) in a C57BL/6 (B6) genetic background (4F mice). We performed doxycycline treatment of 4F mice in 3 different cohorts (Fig. 1a): one cohort was started at 15 months of age and continued until 22 months of age (7-month treatment, ‘long-term’); another was started at 12 months of age and continued until 22 months (10-month treatment, ‘long-term’); and a third one was started at 25 months of age and continued for 1 month (‘short-term’) (Fig. 1a). Control cohorts were untreated 4F young (3 months), 4F old (26 months) and old C57BL/6 (B6) (22 and 25 months) animals, as well as B6 animals treated with a similar doxycycline regimen for 5 months starting at 20 months of age. These cohorts allowed for the assessment of the effects of partial reprogramming on changes that occur as animals age and for the differentiation of any doxycycline-mediated effects from changes elicited by the induction of 4F expression. OSKM expression was detected in different tissues after doxycycline treatment of adult 4F mice (9-month-old mice) (Extended Data Fig. 1).

The long-term expression of reprogramming factors is a concern due to the potential for teratoma formation^{13,14}. This is particularly problematic in aging mice because senescent cell accumulation and associated inflammation can promote cellular reprogramming²¹. However, we did not observe any dramatic change in body weight or survival of 4F mice during doxycycline treatment (Fig. 1b,c). Moreover, complete blood count analysis showed normal white and red blood cells (RBCs) and hemoglobin levels in mice undergoing doxycycline treatment compared to untreated control 4F mice (Fig. 1d). Mice also appeared neurologically normal; open field test analysis to assess exploratory and locomotive behavior at 22 months of age revealed no differences between treatment groups (Fig. 1e).

To determine whether partial reprogramming leads to any histological changes in tissues, we analyzed various tissues collected from 4F and control mice at the end of the treatment and did not observe any gross pathological phenotypes in treated animals (Extended Data Fig. 2). These results indicated that long-term *in vivo* partial reprogramming in WT aging mice does not lead to any overt negative consequences.

Partial reprogramming reverses age-related DNA methylation.

To assess whether these interventions instead would reverse age-related phenotypes in old mice, we first set out to determine the epigenetic age of various tissues using methylation clock analysis^{22,23}. Changes in DNA methylation patterns are a well-established biomarker for aging and several epigenetic clocks have been developed based on these changes to estimate ‘epigenetic age’ independently of chronological age of the animal²³. Such DNA methylation-based epigenetic clocks have also been used to assess the epigenetic age of induced pluripotent stem cells²² and effects of antiaging interventions^{24,25}; a recent study showed that short-term expression of reprogramming factors can reverse the epigenetic clock in human cells¹⁶. To analyze the effects of long-term partial reprogramming on the epigenetic clock of various tissues, we determined DNA methylation patterns and used clocks trained on the relevant tissue types²⁶ (Extended Data Fig. 3). We used new types of epigenetic clocks, Lifespan Uber Correlation (LUC) clocks, which are constructed on the basis of CpGs whose rate of change correlates with maximum life span across mammals²⁷. The LUC clocks revealed a significant reduction of epigenetic age in the kidney and skin (but not other tissues) of long-term partially reprogrammed animals but not in the short-term partially reprogrammed animals (Fig. 2 and Extended Data Figs. 6c). The traditional elastic net clocks also corroborated the rejuvenation effects of partial reprogramming, but mainly in skin (Extended Data Fig. 4, 6a, 6b). In general, the LUC clocks showed a better performance than the traditional elastic net clocks in these partial reprogramming experiments.

Accordingly, across the genome of animals treated long term, but not animals treated short term, CpGs with significantly increased or decreased methylation levels could be identified (Extended Data Figs. 5 and 7). These differentially methylated CpGs were mostly located in exon and intron sequences (Extended Data Figs. 5 and 7), and were often associated with transcriptional changes in nearby genes (Extended Data Fig. 7c). Long-term partial reprogramming was thus sufficient to prevent or reverse age-related DNA methylation changes in skin and kidney, resulting in epigenetic signatures that resembled younger ages. Late-onset, short-term reprogramming, on the other hand, was not sufficient to elicit such changes.

Restoration of transcriptomic signature after partial reprogramming. To further evaluate the nature of cellular changes elicited by partial reprogramming, we performed transcriptome analysis via RNA sequencing (RNA-seq) of each tissue from mice in the various cohorts. In 1-month-treated animals, principal component analysis (PCA) revealed significant differences between young and old tissues but only minor differences between treated and untreated tissues (Fig. 3a–d and Extended Data Fig. 8). This is consistent with the notion that short-term reprogramming in 25-month-old mice is not sufficient to rejuvenate tissues based on methylation clock analysis and was also true when evaluating expression differences in skin specifically (Fig. 3c). Nevertheless, differential gene expression analysis revealed that the number of differentially expressed genes (DEGs) in the skin is much higher when comparing young and old untreated animals than when comparing young untreated with old treated animals, indicating that at least the magnitude of the transcriptional changes in old skin is reversed after short-term treatment (Fig. 3d). Among the genes differentially upregulated after treatment, we observed enrichment of genes involved in hair follicle

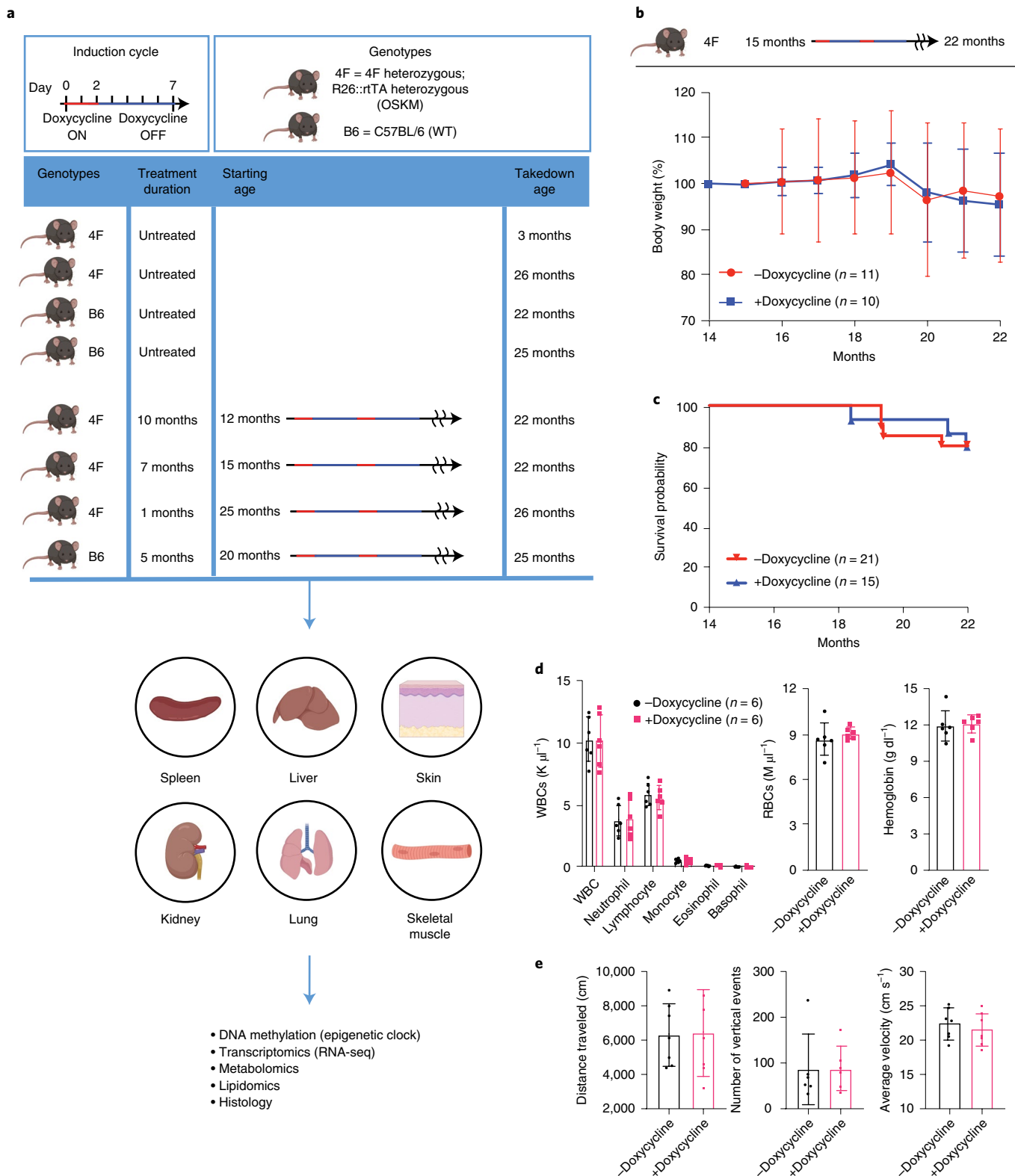


Fig. 1 | Long-term partial reprogramming does not negatively impact health. **a**, Scheme of doxycycline treatment and list of 4F mice included in different cohorts and list of tissues collected for the indicated downstream analysis. **b,c**, Body weight (**b**) and Kaplan-Meier plot of the survival (**c**) of 4F mice during the treatment period. **d**, Complete blood analysis of 4F mice undergoing treatment. The levels of white blood cells (WBCs), RBCs and hemoglobin were measured in the whole blood. **e**, Open field test analysis of 4F mice measured at 22 months of age after 7 months of treatment starting at 15 months of age. $n=6-7$ biological independent mice in each group. For all relevant figures, data are represented as the mean \pm s.d.

development and the hair cycle, while genes involved in interferon responses were selectively downregulated (Fig. 3e and Extended Data Fig. 8c,d). Transcription factor enrichment analysis indicated

a role for oxidative stress regulated factors (nuclear factor erythroid 2-related factor 2) in the differential transcriptome response but also detected the expected enrichment of direct targets of Klf4 and

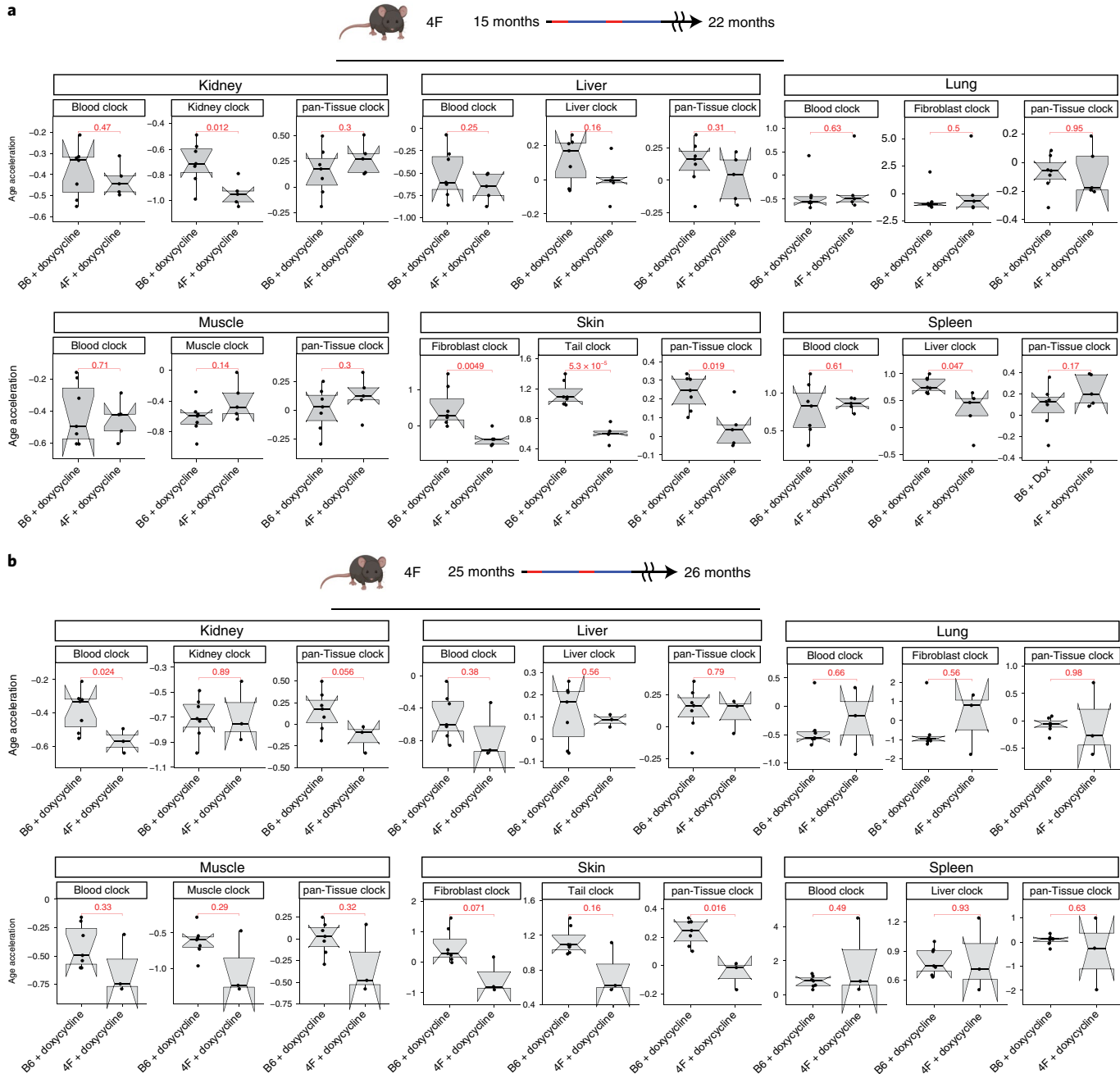


Fig. 2 | Long-term but not short-term partial reprogramming reduces age acceleration in epigenetic clocks in the skin and kidney. **a,b**, Measurement of DNA methylation age acceleration in various tissues of 4F mice using LUC epigenetic clocks trained on the indicated tissues. **a**, DNA methylation age acceleration in 4F mice after 7 months of treatment starting at 15 months of age until 22 months. $n=7$ (B6 + doxycycline) and $n=5$ (4F + doxycycline) biologically independent mice. **b**, DNA methylation age acceleration in 4F mice after 1 month of treatment starting at 25 months of age. $n=7$ (B6 + doxycycline) and $n=3$ (4F + doxycycline) biologically independent mice. Age accelerations are the residuals of the predicted age regressed on the chronological age of each sample. The mean differences were examined by a two-sided Student's *t*-test of age acceleration differences between the groups. *P* values are reported in each panel. The boxes show the interquartile range (IQR) of the age accelerations. The notches indicate the 95% confidence interval of the median. The whiskers represent the 1.5× IQR length of the age accelerations.

c-Myc (Extended Data Fig. 8e). While transcriptome changes were small overall, the differential expression of stress and inflammation genes suggested that even short-term reprogramming may have had beneficial consequences in the skin of old mice.

The transcriptome changes were more evident after long-term reprogramming, which is consistent with the methylation clock analysis (Fig. 4a,b and Extended Data Fig. 9). In the skin, for example, we observed a clear separation of skin samples from

control and doxycycline-treated mice (Fig. 4c and Extended Data Fig. 9e). Differentially induced genes included genes involved in metabolism and oxidative phosphorylation, while genes involved in inflammation and senescence were downregulated (Fig. 4d,e and Extended Data Fig. 9). Importantly, long-term doxycycline treatment of WT (B6) mice only elicited minor transcriptome changes, indicating that most of the observed changes were a consequence of 4F transgene expression (Extended Data Fig. 9f).

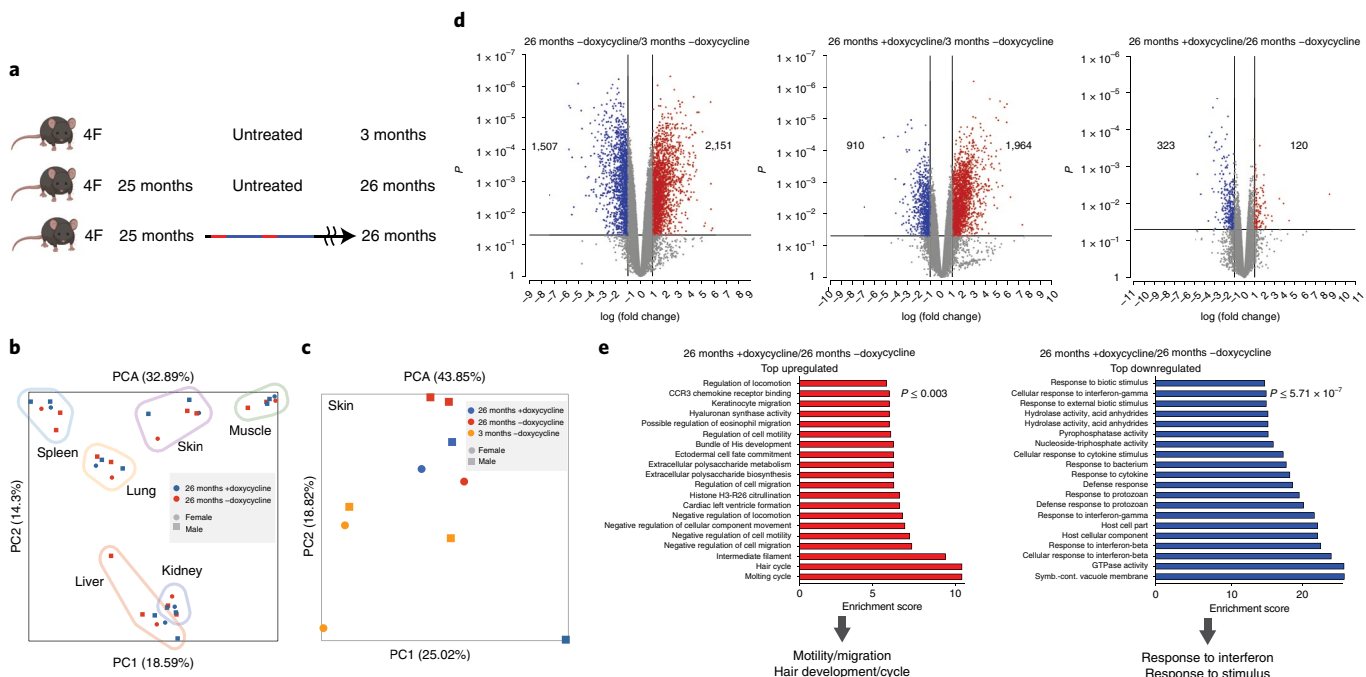


Fig. 3 | Short-term partial reprogramming reduces interferon response gene induction in the skin and restores hair cycle gene expression.

a, Transcriptional profiling of 25-month-old 4F mice after 1 month of treatment by comparison with untreated 4F and young 4F mice (3 months). $n=4$ (old 4F – doxycycline), $n=3$ (old 4F + doxycycline) and $n=4$ (young 4F – doxycycline) biologically independent mice. **b**, Plot of principal components (PC1 and PC2) obtained from the PCA of tissues from control and treated 4F male and female mice at 26 months of age. **c**, Plot of principal components (PC1 and PC2) of skin from 26-month-old (control and treated) and 3-month-old 4F mice. **d**, Volcano plots of RNA-seq data of skin generated by comparing 26-month-old (control and treated) and 3-month-old 4F mice. **e**, Gene Ontology (GO) analysis of RNA-seq data of skin showing the top upregulated and downregulated genes. The DEG list cutoffs were defined as $P < 0.05$ and a log(fold change) of 2. Symb.-cont., Symbiont-containing.

When we compared DEGs in the skin across cohorts, we found that the two long-term treatment regimens (seven and ten months) overlapped significantly, while short-term treatment (and control treatments) had a distinct pattern of DEGs (Fig. 4f). The genes uniquely induced in the two long-term treatment regimens included genes involved in lipid and fatty acid metabolism, while uniquely downregulated genes included genes involved in epidermal differentiation. These observations suggested that long-term reprogramming of the skin may contribute to the preservation of a more plastic, less differentiated state in old skin cells. To test this idea, we examined whether long-term partial reprogramming maintained the proliferative capacity of epidermal cells by staining for the proliferation marker protein Ki67 (Extended Data Fig. 10). As previously observed in progeria models¹⁵, the proliferation rates of cells in the skin of 4F mice undergoing doxycycline treatment were indeed higher than in control mice, both after short- and long-term reprogramming (Extended Data Fig. 10a,b). Consistent with more proliferation in the skin, the thickness of the skin epidermis in female mice was higher in 4F mice that had undergone long-term partial reprogramming compared to the skin of untreated mice (Extended Data Fig. 10c).

Improved regenerative capacity of skin after in vivo partial reprogramming. We asked whether this increase in proliferation in the skin may also influence wound healing capacity. The regenerative capacity of several tissues declines with age^{28–30} and 4F reprogramming may specifically influence regenerative processes by impacting the niche or the stem cells of specific tissues^{20,31}. In the skin, wound healing encompasses the formation of scar tissue, which consists of an increased collagen-rich matrix. We performed skin injury in mice after long-term partial reprogramming to measure

the changes in wound repair. In humans, wounds are healed by the generation of new tissue; in rodents, skin contraction facilitates wound healing. For this reason, we used an excisional wound splinting model, where a splinting ring prevents the contraction of the surrounding skin area and enables wound healing by reepithelialization (Fig. 5a). At the time of the experiment, mice were not dosed with doxycycline to avoid any effects of reprogramming factors on the wound healing process. We did not observe any notable differences in the closure rate of the wound surface and gross morphology of the wound between treated and untreated mice (Fig. 5b). However, increased proliferative capacity of epidermal cells was observed in the wound areas of long-term partially reprogrammed mice compared to untreated mice (Fig. 5c,d). An increase in tissue fibrosis was observed with age in different tissues due to inflammation and chronic insults. A similar phenomenon was observed after wound healing. To find out whether 4F reprogramming may reduce tissue fibrosis in this context, we analyzed fibrotic tissue accumulation in the skin wound after healing (Fig. 5e,f). We observed an increase in collagen deposits in the wound area of old untreated mice, whereas in long-term partially reprogrammed mice, fibrosis in the wound area was low and similar to young mice. Additionally, we performed muscle injury using cardiotoxin in mice after long-term partial reprogramming. We did not observe any significant changes (muscle fiber size and PAX7⁺ stem cells) in the regenerative potential between control and doxycycline-treated mice (Extended Data Fig. 10d,e). In our long-term experiments, doxycycline delivered in drinking water did not induce higher levels of 4F expression in the muscle to prevent age-associated decline of muscle regeneration. Overall, these results demonstrate that long-term partial reprogramming improves wound healing, resulting in a reduction in the accumulation of fibrotic tissue in the wound area.

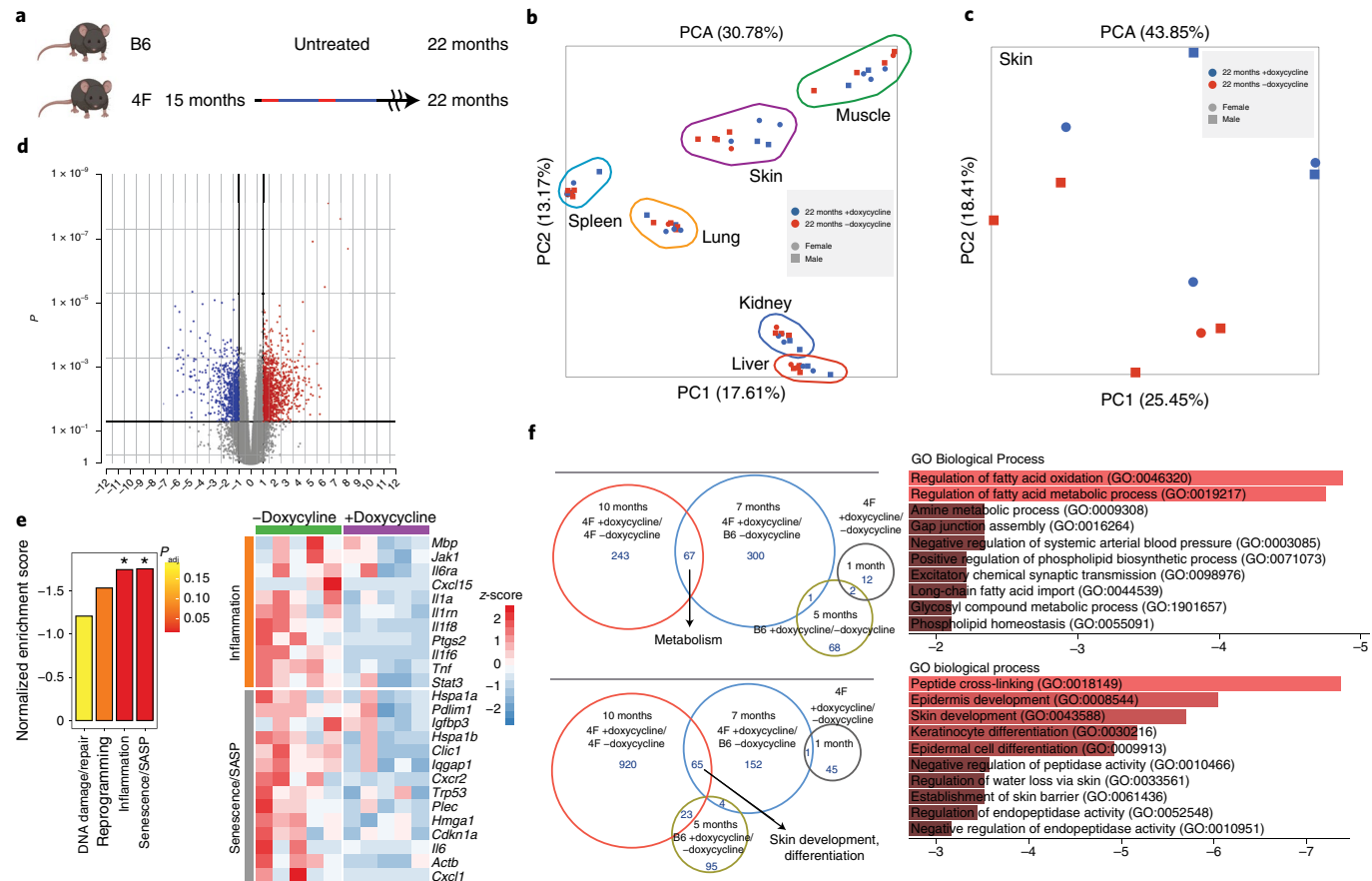


Fig. 4 | Long-term reprogramming restores metabolic gene expression and reduces inflammatory/SASP gene expression. **a**, Transcriptional profiling of 22-month-old 4F mice after 7 months of treatment by comparison with untreated B6 mice. $n=5$ (B6 – doxycycline) and $n=5$ (4F + doxycycline) biologically independent mice. **b**, Plot of the principal components (PC1 and PC2) obtained from the PCA of tissues from control and treated 4F male and female mice at 22 months of age. **c**, Plot of the principal components (PC1 and PC2) of skin from 22-month-old mice (control and treated). **d**, Volcano plot of skin RNA-seq data generated by comparing control and treated mice. **e**, Downregulation of senescence and inflammatory genes in the skin of treated mice compared to control mice. **f**, Venn diagram showing the common genes involved in metabolism and skin development in 7- and 10-month-treated mice. The DEG list cutoffs are defined as $P < 0.05$ and a log(fold change) of 2.

Partial reprogramming restores metabolomic and lipidomic profiles. To gain an insight into the systemic changes elicited in mice by long-term partial reprogramming, we performed untargeted metabolomic and lipidomic profiling of serum from mice from the 10-month-treated cohort at 17 months of age (that is, 5 months after treatment onset) and at 22 months of age (that is, at the end of treatment) (Fig. 6a). Consistent with the transcriptome and methylation analysis, we observed only minor changes after 5 months of treatment, while major age-related metabolite changes in the serum were reversed after long-term reprogramming at the 22-month time point (Fig. 6b). Among the polar metabolites whose age-related changes were reversed, metabolite intermediates of one-carbon metabolism were prominent, including S-adenosyl methionine, 1-methylguanine, 1-methyladenosine, dimethyllysine and trimethyllysine (Fig. 6d,e). These metabolites are also elevated in progeria mice and their restoration to more youthful levels may thus reflect overall rejuvenation of the animals' physiology³². Similarly, reversion of age-related elevation of hydroxyproline and oxoprolidine may reflect a reversion of fibrosis in partially reprogrammed mice. Among the nonpolar metabolites, significant age-related elevation of triacylglycerides and reduction of phospholipids were reversed by partial reprogramming, highlighting the impact of partial reprogramming on overall metabolic homeostasis in aged mice (Fig. 6c,d). Importantly, control WT animals exposed to a similar

regimen of doxycycline treatment exhibited no major changes in metabolites (Fig. 6b,c). Altogether, this metabolomics analysis further supports the notion that short-term reprogramming has only minor consequences (at least at mid-age), while long-term reprogramming reverses or prevents major age-related changes in animal physiology.

Discussion

Our results demonstrate that partial reprogramming can be performed in aging WT mice for extended periods without obvious adverse effects. Partial reprogramming prevented the manifestation of age-associated histological changes and maintained cell proliferation in tissues such as the skin. The changes in DNA methylation and gene expression observed in the skin and kidney are consistent with the idea that partial reprogramming can prevent the establishment of aging phenotypes or even rejuvenate tissues, as predicted by similar results in various other models^{16–18}. Interestingly, our data also indicate that short-term late-onset reprogramming may not be sufficient to elicit similar molecular changes reminiscent of rejuvenation, although the transcriptional response seems to indicate a reduction in stress pathway activation. It is possible that the initial transcriptional response is transient and is only captured in more permanent epigenetic changes after additional rounds of 4F expression. It is also possible that at 25 months of age, mice have

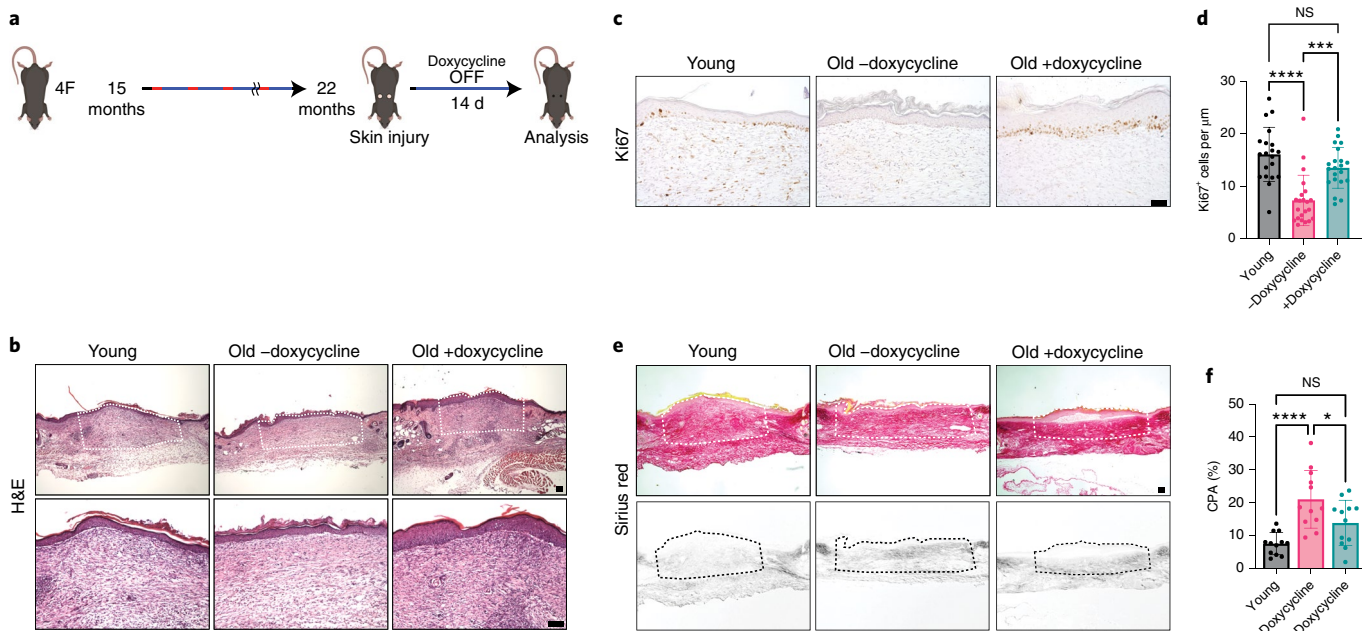


Fig. 5 | Long-term reprogramming reduces fibrotic tissue formation during wound healing in the skin. **a**, Excisional wound splinting model in long-term partial reprogrammed mice at 22 months of age and young 4F mice (3 months). Wound healing was analyzed 14 d after the injury in female mice. Mice were not treated with doxycycline during the repair period. **b**, Representative images of histological analysis of wound area by H&E staining. The dotted lines represent the wound area. Bottom: Higher magnification of the wound area. Scale bar, 100 μm . **c**, Representative images of immunostaining of Ki67⁺ cells in the epidermis of the wound area. $n=3$ biologically independent mice (3 sections per mice were used for quantification). **d**, Quantification of Ki67⁺ cells in the epidermis of the wound area. $n=3$ biologically independent mice (3 sections per mice were used for quantification). **e**, Sirius Red staining of the wound area. Top: Bright field images. Bottom: Images obtained with polarized light. The dotted lines represent the wound area. Scale bar, 100 μm . **f**, Quantification of collagen proportionate area (CPA) in the wound area. $n=4$ biologically independent mice (3 sections per mice were used for quantification). For all relevant figures, data are presented as the mean \pm s.d. * $P<0.05$, ** $P=0.0001$ and *** $P<0.0001$ according to a one-way ANOVA with Bonferroni correction.

acquired irreversible aging phenotypes in various tissues. Future studies will have to establish the threshold at which transient stress reduction may transition into more permanent rejuvenation during 4F reprogramming.

While our metabolomics analysis of serum indicates that long-term partial reprogramming has widespread physiological effects, it was striking that methylation and transcriptome analysis indicated more significant reduction in molecular aging phenotypes in the skin and kidney than in other tissues. It is unclear why these tissues may be more susceptible to OSKM rejuvenation. Based on our analysis of OSKM factor expression levels, these differences do not seem to be a consequence of different transgene expression levels. An intriguing hypothesis is thus that the skin and kidney are more susceptible to reprogramming than other tissues, an observation that may be a consequence of differences in epigenetic status. Further detailed transcriptomic and epigenetic analyses of various tissues at the single-cell level to determine changes in cell composition after reprogramming, as well as more comprehensive titration of OSKM delivery to various tissues, may provide answers to this question. Furthermore, it is important to evaluate possible sexual dimorphism in response to 4F reprogramming *in vivo*. Our data suggest that the skin of female mice responds to reprogramming more effectively than the skin of male mice. Whether this is a consequence of the transgenes used or a more general difference between sexes will have to be assessed.

The reversion of age-related systemic physiological changes revealed by metabolomic and lipidomic analyses indicates a broader beneficial outcome of long-term 4F reprogramming in mice. Exploring the specific mechanisms by which one-carbon metabolism and/or the balance between serum triacylglycerides and phospholipids are affected, will be particularly interesting in future studies.

Our results collectively demonstrate that *in vivo* partial reprogramming can lead to beneficial effects in WT aging mice by reversing or preventing epigenetic changes associated with biological aging. Based on our observations in metabolomics experiments, it is likely that long-term reprogramming prevents the establishment of systemic age-associated phenotypes, although we cannot rule out that a reversion of aging phenotypes is possible when 4F reprogramming is applied in a ‘window of opportunity’ between 22 and 25 months of age. Our data further suggest that the duration of treatment determines the extent of changes in specific tissues and organs, as well as systemically. However, late short-term reprogramming of older animals may not achieve rejuvenation because cells have entered a ‘refractory’ or ‘senescent’ state that prevents reprogramming.

The relationship between cellular senescence and reprogramming is likely to be complex. While senescent cells themselves may be difficult to reprogram, senescent cells also influence their microenvironment by secreting cytokines and growth factors. This ‘senescence-associated secretory phenotype’ (SASP) has been described as a facilitator of reprogramming²¹; it will be interesting to further explore the relationship between reprogramming and senescence in a broader tissue-specific manner. Together with other recent findings^{16–19}, our data support the notion that partial 4F reprogramming may constitute an organismal rejuvenation intervention and strategy to alleviate the manifestation of age-associated diseases.

Methods

Animal use and care. All animal procedures were performed according to National Institutes of Health (NIH) guidelines and approved by the Committee on Animal Care at the Salk Institute. Mice carrying the OSKM polycistronic cassette and rtTA were obtained from The Jackson Laboratory (stock no. 011011). All the experiments were performed in male and female mice carrying one copy of

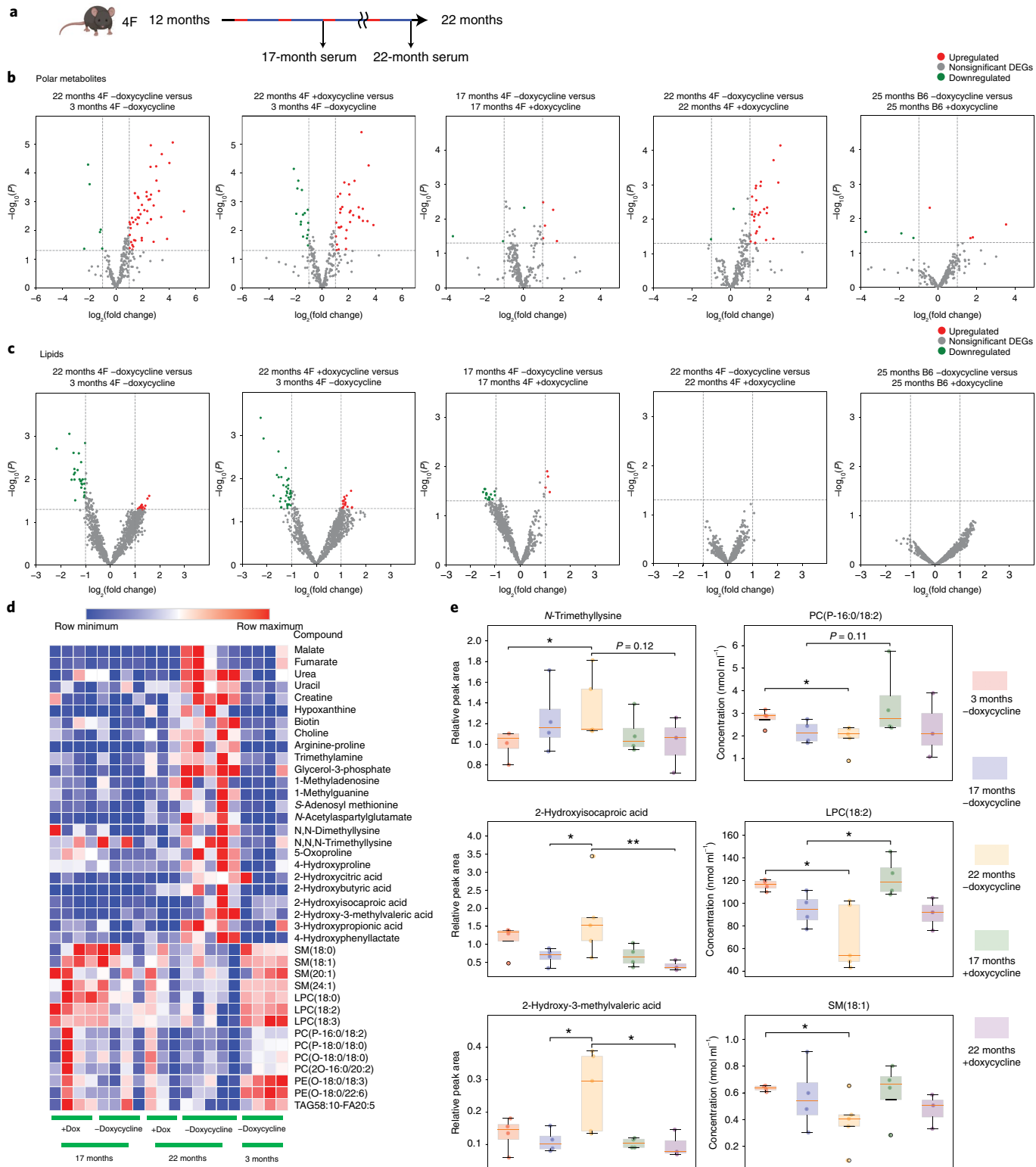


Fig. 6 | Restoration of metabolomic and lipidomic profile in the serum following long-term partial reprogramming. **a**, Global metabolomic and lipidomic profiles were obtained from the serum of 4F mice after five and ten months of treatment, respectively. **b,c**, A total of 279 metabolites (**b**) and 1,070 lipids (**c**) were identified and analyzed with complementary LC-MS methods, respectively. The volcano plots show the pairwise comparison of different age and treatment groups for metabolomics and lipidomics data. **d**, Heatmap listing a combined group of metabolites and lipids that demonstrate the metabolic landscape change during the aging process, as well as the reversal effect on 4F treatment. **e**, Six compounds as aging classifiers that appeared to go back to a younger level with 4F induction. In the boxplot, the y axis of the metabolites refers to relative quantification results, that is, the LC-MS peak area ratio of analyte to the corresponding stable isotope-labeled internal standard; the y axis of lipids refers to the concentration value of the absolute quantification results. The boxplots show the median (middle line), 25th and 75th percentiles (box) and 5th and 95th percentiles (whiskers) as well as the maximum and minimum (single points). * $P < 0.05$, ** $P < 0.01$ according to a one-way ANOVA with Bonferroni correction. $n = 4$ (3M, 17 months -doxycycline and 17 months +doxycycline), $n = 5$ (22 months -doxycycline) and $n = 3$ (22 months +doxycycline) biologically independent mice.

the OSKM polycistronic cassette and the rtTA. All the mice were in a C57BL/B6 background. The mice were housed in a temperature-controlled room ($22 \pm 1^\circ\text{C}$) at 40–60% humidity with a 12-h light and dark cycle between 6:00 and 18:00 and free access to water and food (laboratory diet no. 5053). The induction of OSKM was performed by administering doxycycline (1 mg ml⁻¹; Sigma-Aldrich) in drinking water for 2 d followed by 5 d of withdrawal per week until the end of the experiment. Blood samples from the mice were collected by submandibular bleeding. All the tissue samples from the mice were collected 5 d after stopping the doxycycline treatment. The age and number of mice used in each experiment are reported in the figure legends.

Behavioral testing was carried out at the Salk Institute for Biological Studies Behavioral Testing Core. The open field test measured the baseline levels of locomotor activity in freely moving mice. Mice were individually placed into clear Plexiglas boxes (40.6 × 40.6 × 38.1 cm) surrounded by multiple bands of photo beams and optical sensors that measured horizontal (ambulatory) and vertical (rearing) activity (Med Associates). Their movement was detected as breaks within the beam matrices and automatically recorded for 60 min.

Wound healing model. An excisional wound splinting model was generated in aged 4F mice according to the previously described procedure³³. Briefly, 15-mm diameter circular splint rings made from a 0.5-mm thick silicone sheet with a hole in the center were made using a 6-mm biopsy punch. The splints were sterilized by washing with detergent, sodium hypochlorite and 70% ethanol with washes in sterile water in between. After the final wash in 70% ethanol, the splints were air-dried in a tissue culture hood and stored in a sterile bottle. Next, the dorsal side of the mice was shaved and disinfected. The dorsal skin from the midline was pulled with figures and a 5-mm diameter biopsy punch was punched through the folded skin to create two symmetrical excisional wounds on either side of the midline. Then, instant bonding glue was spread on one side of the splint and placed around the wound with the center covering the wound area. The splints were secured to the skin with four interrupted sutures. The wounds and splints were covered with Tegaderm sterile transparent dressing (3M) and the wound was carefully dressed with a self-adhesive elastic bandage, avoiding restriction of breathing and movement of mice. Mice were housed individually in the cages. The skin surrounding the wound area was collected after 14 d and fixed in 4% paraformaldehyde (PFA), followed by embedding in optimal cutting temperature compound.

Muscle injury model. Muscle injury was performed by intramuscular injection of 40 µl cardiotoxin (10 µM; Latoxin) in the tibialis anterior muscle. Ten days after cardiotoxin-induced muscle injury, mice were killed and the tibialis anterior muscles were dissected and processed for histological analysis.

Histological analysis. The mice tissue samples were collected at the end of treatment, at 22 or 26 months of age. The tissues from 3-month-old mice were used as young controls. The tissues were fixed in 4% PFA overnight and embedded in paraffin. The paraffin sections were used for hematoxylin and eosin (H&E) staining. The H&E images were captured with an Olympus IX51 microscope.

Immunohistochemistry. Paraffin sections underwent antigen retrieval using HistovT One (Nacalai Tesque) after deparaffinization and rehydration steps. The tissue sections were incubated with anti-Ki67 (1:200 dilution; catalog no. 9027; Cell Signaling Technology), anti-Pax7 (1:200 dilution; catalog no. Pax7-c; DSHB) or anti-Dystrophic (1:500 dilution; catalog no. ab15277; Abcam) primary antibody in donkey serum overnight. For the Ki67 staining, sections were incubated with ImmPRESS reagent (Vector Laboratories) for 30 min and positive cells were visualized with ImmPACT DAB substrate (Vector Laboratories). Positive cells were quantified from more than three sections from three animals with ImageJ (FIJI) software version 2.1.0/1.53c (NIH). For Pax7 and dystrophin staining, sections were incubated with respective secondary antibodies (1:500 dilution) goat anti-mouse IgG2b (Alexa Fluor 488, catalog no. A21141; Invitrogen) and goat anti-mouse IgG2b (Alexa Fluor 647, catalog no. A21242; Invitrogen) with 4',6-diamidino-2-phenylindole for 1 h at room temperature. Fluorescent images were captured using a Zeiss LSM 710 laser scanning confocal microscope.

RNA extraction and standard input RNA-seq. The QIAGEN RNeasy Kit was used to extract RNA from several tissues with few modifications. RNA was extracted from fresh tissues using TRIzol and chloroform. The aqueous phase was mixed with an equal volume of 100% ethanol and then loaded onto the QIAGEN columns and followed the manufacturer's protocol (DNA digestion performed on column).

Total RNA was quantified with the Qubit RNA HS Assay Kit (Thermo Fisher Scientific) and quality was assessed using RNA ScreenTape on a 4200 TapeStation (Agilent Technologies). To generate the sequencing library, the TruSeq Stranded mRNA Kit (Illumina) was used with an input of 100 ng of total RNA. Libraries were quantified with the Qubit dsDNA HS Assay Kit (Thermo Fisher Scientific) and the average library size was determined using D1000 ScreenTape on a 4200 TapeStation. Libraries were pooled and sequenced on the NovaSeq 6000 system (Illumina) to generate 30 million single-end 50-base paired reads for each sample.

Transcription profiling. RNA-seq alignment and analysis. Sequencing reads were filtered and aligned with HTSeqGenie v4.2.1 or v4.4.1 (ref. ³⁴). GSNAP v.2013-11-01 was used for alignment, through the HTSeqGenie wrapper, against the GENCODE Basic gene model on the mouse genome assembly GRCm38 before importing into the Partek Flow Genomic Analysis software version 2.3. Only reads with unique genomic alignments were analyzed. Analysis and visualization was performed in R version 4.0.0 (<https://www.r-project.org/>). Differential gene expression was calculated using voom+limma version 3.44.3³⁵, with trimmed mean of M-values normalization and multiple hypothesis correction of P values performed using the Benjamini-Hochberg method. Gene set enrichment analysis was performed using the fgsea v.1.12.0 R package³⁶ with default parameters. For transcription factor target enrichment, gene sets were provided by the TRANSFAC Predicted Transcription Factor Targets database version January, 2021³⁷ available on Harmonizome (<https://maayanlab.cloud/Harmonizome>)³⁸. A manually curated gene set was used to calculate the enrichment of inflammatory and SASP gene sets.

The Partek Flow Genomic Analysis software was used to perform the PCA and for differential gene expression analysis. DEG lists were filtered based on $P < 0.05$. Gene set enrichment analysis was performed using Partek Flow Genomic Analysis or Enrichr version 2021 (<https://maayanlab.cloud/Enrichr>) (Figs. 3 and 4 and Extended Data Fig. 9). Venn diagrams in Fig. 4 were produced using DeepVenn (<https://www.deepvenn.com/>) by comparing significant DEG lists for the various cohorts. To exclude any doxycycline-specific effects, –doxycycline versus +doxycycline C57BL/B6 were compared to the experimental cohorts. Overlapping gene lists between long-term-treated cohorts were analyzed with Enrichr, focusing on 'GO Biological Process'.

DNA methylation analysis. All methylation data were generated using a custom Illumina methylation array (HorvathMammalMethylChip40) based on 37,492 CpG sites. Out of these 37,492 sites, 1,986 were selected based on their utility for human biomarker studies. The remaining CpGs were chosen due to their location in stretches of DNA that are highly conserved across mammalian species³⁹. The particular subset of species for each probe is provided in the chip manifest file at the National Center for Biotechnology Information Gene Expression Omnibus (GEO) platform ([GPL28271](https://www.ncbi.nlm.nih.gov/geo/query/acc.cgi?acc=GPL28271)). SeSAMe normalization was used to define the Beta values for each probe⁴⁰.

The LUC clocks were developed in a separate training set²⁷. Technically, LUC clocks are defined as ridge regression models where chronological age (dependent variable) was regressed on 629 selected CpGs whose intraspecies age correlates with maximum life span across mammalian species. The different LUC clocks were defined with respect to different training sets. For example, the liver LUC clock was only trained in mouse liver samples. Eleven tissue-specific LUC clocks and 1 pan-Tissue LUC clock were developed for mice²⁷. Our analysis used the most relevant clocks for each target tissue. To arrive at an unbiased measure of epigenetic age acceleration, we defined the latter as raw residuals resulting from regressing predicted age on actual chronological age, that is, age acceleration = residuals (predicted age ~ age). The treatment effect on age accelerations was assessed by a linear regression model: age acceleration ~ treatment.

Metabolomics and lipidomics analyses. Chemicals and reagents. The following reagents and authentic standard compounds were obtained from the named suppliers: water, methanol and acetonitrile (liquid chromatography–mass spectrometry (LC–MS) grade; Fisher Chemical); chloroform (American Chemical Society grade; Sigma-Aldrich); dichloromethane (DCM; Honeywell Burdick & Jackson); Lipidizer Platform internal standards kit (SCIELEX); in-house metabolomics Recovery IS mixture (deoxycholic acid-d4, glutamate-d3, adenosine monophosphate-¹³C10); in-house metabolomics Global IS mixture (cholic acid-d4, glycocholic acid-d4, tryptamine-d4, glutamine-d5, malic acid-d3, nicotinic acid-d4, glucose 6-phosphate-¹³C6 and stable isotope-labeled amino acid mixture kit purchased from Sigma-Aldrich).

Sample preparation and extraction. All sample preparation procedures were kept on dry ice. Briefly, 350 µl cold methanol containing the in-house metabolomics Recovery IS mixture, 200 µl cold chloroform and 100 µl cold Lipidizer IS were added to each 35 µl mouse serum aliquot. Samples were vortexed for 10 s, incubated on dry ice for 5 min and centrifuged at 4,000 r.p.m. for 5 min. Supernatants were transferred to a clean tube and 200 µl cold H₂O were added to perform liquid–liquid phase separation. Samples were mixed and centrifuged again. The top layer aliquots were transferred, dried and reconstituted in 100 µl acetonitrile:water (8:2, v/v) containing the in-house metabolomics Global IS mixture and submitted for metabolomics analysis. The bottom layer aliquots were transferred, dried and reconstituted in 300 µl DCM:methanol (1:1, v/v) containing 10 mM ammonium acetate and submitted for lipidomics analysis.

LC–MS analysis for metabolomics. Metabolomics data for mouse serum were acquired using three complementary LC–MS analytical assays. An ACQUITY UPLC BEH amide column (2.1 mm × 150 mm × 1.7 µm, 130 Å; Waters Corporation) was used to separate polar metabolites with mobile phase A of 100% H₂O containing 10 mM ammonium formate and 0.125% formic acid, and mobile phase B of 95% acetonitrile in H₂O containing 10 mM ammonium formate and 0.125% formic

acid. A Phenomenex Luna NH2 HPLC column (2 mm × 250 mm × 3 μm, 100 Å; Phenomenex) was used to separate highly polar metabolites and sugar phosphates with a mobile phase A of H₂O-ACN (95:5, v/v) containing 20 mM ammonium hydroxide and 20 mM ammonium acetate, and mobile phase B of 100% acetonitrile only. Additionally, a derivatization assay targeting short-chain fatty acids was performed with details reported previously¹¹. All data acquisition was achieved on a Shimadzu Nexera HPLC series system coupled with a Thermo Q Exactive Plus Hybrid Quadrupole-Orbitrap Mass Spectrometer (Thermo Fisher Scientific). An injection volume of 3 μl was used for sample analysis under heated electrospray ionization. Samples were run for both positive and negative mode for the BEH amide assay, negative only mode for the Luna NH2 assay and positive only mode for the derivatization assay. The Q Exactive Plus mass spectrometer was operated with the following parameters: sheath gas flow rate, 50 units; aux gas flow rate, 13 units; aux gas temperature, 425 °C; capillary temperature, 263 °C; spray voltage, 3,500 V for positive and −2,500 V for negative; scan mode, full MS scan with data-dependent MS-MS acquisition. In full MS scan, the scan range was 60–900 m/z; resolution was 70,000; the AGC target was 1 × 10⁶; and the maximum IT was 200 ms. In the ddMS2 scan, the top 5 ions were selected with an isolation window of 1.5 m/z; resolution was 17,500; the AGC target was 5 × 10⁴; and the maximum IT was 20 ms. The data acquisition software Xcalibur version 4.2 (Thermo Fisher Scientific) was used to collect the raw metabolomics dataset.

LC-MS analysis for lipidomics. The lipidomics data for the mouse serum were acquired using two complementary LC-MS analytical assays. For most of the lipid species, direct infusion analysis was performed on a QTRAP 6500 mass spectrometer (SCIEX) coupled to a SelexION differential mobility system (SCIEX) and Lipidzyer platform. Additionally, an XBridge BEH amide column (4.6 mm × 150 mm × 3.5 μm, 130 Å; Waters Corporation) was used to separate PC ether lipids with a mobile phase A of ACN-H₂O (95:5, v/v) containing 1 mM ammonium acetate and a mobile phase B of ACN-H₂O (50:50, v/v) containing 1 mM ammonium acetate. This analysis was performed on a QTRAP 6500+ mass spectrometer (Applied Biosystems) under negative ionization mode with following source settings: turbo ion spray source at 550 °C; N₂ nebulization gas at 50 psi; N₂ heater gas at 60 psi; and curtain gas at 35 psi. Collision-activated dissociation gas pressure was held at medium, turbo ion spray voltage at −4,500 V, declustering potential at −80 V, entrance potential at −10 V, collision cell exit potential at −10 V and collision energy at −50 units. Data were collected in multiple reaction monitoring mode with transitions employed as their acetic acid adducts to the fatty acyl chains.

Data processing. The data processing software Compound Discoverer version 3.1 (Thermo Fisher Scientific), TraceFinder version 4.1 (Thermo Fisher Scientific) and Polly platform version 1 (ElucidaCorporation) were used for metabolite identification, peak picking and peak integration and statistical analysis, respectively. Metabolites were identified at level 1 confidence⁴² by matching at least 2 independent orthogonal experimental data (accurate mass, isotopic ratio, retention time and MS-MS fragmentation pattern) against an in-house compound RT library, open access mass spectral repository (MassBank of North America; <https://mona.fiehnlab.ucdavis.edu/>)⁴³ and commercial mzCloud (Thermo Fisher Scientific) mass spectral database version 2021. Trend analysis of stable isotope-labeled internal standards and matrix PoolQC samples were examined to validate system suitability and data robustness. For the metabolomics results, relative quantification was obtained through either MS peak area of the analyte or MS peak area ratio of analyte/internal standard. For the lipidomics results, absolute quantification (concentration) was obtained with the MultiQuant software version 3.0.2 (SCIEX) and Lipidzyer platform. To exclude the doxycycline effects, C57BL/B6 – doxycycline versus C57BL/B6 + doxycycline were compared using a Limma test (*P* values and log₂(fold changes) are shown in Supplementary Table 6). Metabolites that changed significantly were excluded; metabolites included in the 4F comparison did not show significant changes between C57BL/B6 – doxycycline versus C57BL/B6 + doxycycline.

Statistics. Statistical analyses were performed with Prism 8 (GraphPad Software). Statistical analyses of multiple groups were performed by one-way analysis of variance (ANOVA) with Bonferroni correction. For statistical comparison of two groups, we used a two-tailed Student's *t*-test. A value of *P*<0.05 was considered significant.

Reporting Summary. Further information on research design is available in the Nature Research Reporting Summary linked to this article.

Data availability

DNA methylation and RNA-seq data are deposited in the GEO under the accession no. [GSE190665](https://www.ncbi.nlm.nih.gov/geo/query/acc.cgi?acc=GSE190665) and the SuperSeries under accession no. [GSE190986](https://www.ncbi.nlm.nih.gov/geo/query/acc.cgi?acc=GSE190986). The metabolomics and lipidomics raw data can be found in Supplementary Tables 8 and 9 (4F mice serum) and 10 and 11 (B6 mice serum). Other data supporting the findings of the study can be requested from the corresponding author.

Received: 24 February 2021; Accepted: 26 January 2022;
Published online: 7 March 2022

References

- Ermolaeva, M., Neri, F., Ori, A. & Rudolph, K. L. Cellular and epigenetic drivers of stem cell ageing. *Nat. Rev. Mol. Cell Biol.* **19**, 594–610 (2018).
- Keenan, C. R. & Allan, R. S. Epigenomic drivers of immune dysfunction in aging. *Aging Cell* **18**, e12878 (2019).
- Melzer, D., Pilling, L. C. & Ferrucci, L. The genetics of human ageing. *Nat. Rev. Genet.* **21**, 88–101 (2020).
- Campisi, J. et al. From discoveries in ageing research to therapeutics for healthy ageing. *Nature* **571**, 183–192 (2019).
- Smith, H. J., Sharma, A. & Mair, W. B. Metabolic communication and healthy ageing: where should we focus our energy? *Dev. Cell* **54**, 196–211 (2020).
- Zhang, W., Qu, J., Liu, G.-H. & Belmonte, J. C. I. The ageing epigenome and its rejuvenation. *Nat. Rev. Mol. Cell Biol.* **21**, 137–150 (2020).
- Mahmoudi, S., Xu, L. & Brunet, A. Turning back time with emerging rejuvenation strategies. *Nat. Cell Biol.* **21**, 32–43 (2019).
- Mahmoudi, S. & Brunet, A. Aging and reprogramming: a two-way street. *Curr. Opin. Cell Biol.* **24**, 744–756 (2012).
- Takahashi, K. & Yamanaka, S. Induction of pluripotent stem cells from mouse embryonic and adult fibroblast cultures by defined factors. *Cell* **126**, 663–676 (2006).
- Liu, G.-H. et al. Recapitulation of premature ageing with iPSCs from Hutchinson–Gilford progeria syndrome. *Nature* **472**, 221–225 (2011).
- Zhang, J. et al. A human iPSC model of Hutchinson Gilford progeria reveals vascular smooth muscle and mesenchymal stem cell defects. *Cell Stem Cell* **8**, 31–45 (2011).
- Lapasset, L. et al. Rejuvenating senescent and centenarian human cells by reprogramming through the pluripotent state. *Genes Dev.* **25**, 2248–2253 (2011).
- Abad, M. et al. Reprogramming in vivo produces teratomas and iPS cells with totipotency features. *Nature* **502**, 340–345 (2013).
- Ohnishi, K. et al. Premature termination of reprogramming in vivo leads to cancer development through altered epigenetic regulation. *Cell* **156**, 663–677 (2014).
- Ocampo, A. et al. In vivo amelioration of age-associated hallmarks by partial reprogramming. *Cell* **167**, 1719–1733.e12 (2016).
- Sarkar, T. J. et al. Transient non-integrative expression of nuclear reprogramming factors promotes multifaceted amelioration of aging in human cells. *Nat. Commun.* **11**, 1545 (2020).
- Lu, Y. et al. Reprogramming to recover youthful epigenetic information and restore vision. *Nature* **588**, 124–129 (2020).
- Doers, M. C., Schöler, H. R. & Wu, G. Reduction of fibrosis and scar formation by partial reprogramming in vivo. *Stem Cells* **36**, 1216–1225 (2018).
- Rodríguez-Matellán, A., Alcazar, N., Hernández, F., Serrano, M. & Ávila, J. In vivo reprogramming ameliorates aging features in dentate gyrus cells and improves memory in mice. *Stem Cell Rep.* **15**, 1056–1066 (2020).
- Wang, C. et al. In vivo partial reprogramming of myofibers promotes muscle regeneration by remodeling the stem cell niche. *Nat. Commun.* **12**, 3094 (2021).
- Mosteiro, L. et al. Tissue damage and senescence provide critical signals for cellular reprogramming in vivo. *Science* **354**, aaf4445 (2016).
- Horvath, S. DNA methylation age of human tissues and cell types. *Genome Biol.* **14**, 3156 (2013).
- Horvath, S. & Raj, K. DNA methylation-based biomarkers and the epigenetic clock theory of ageing. *Nat. Rev. Genet.* **19**, 371–384 (2018).
- Wang, T. et al. Epigenetic aging signatures in mice livers are slowed by dwarfism, caloric restriction and rapamycin treatment. *Genome Biol.* **18**, 57 (2017).
- Maegawa, S. et al. Caloric restriction delays age-related methylation drift. *Nat. Commun.* **8**, 539 (2017).
- Thompson, M. J. et al. A multi-tissue full lifespan epigenetic clock for mice. *Aging (Albany NY)* **10**, 2832–2854 (2018).
- Haghani, A. et al. Divergent age-related methylation patterns in long and short-lived mammals. Preprint at [bioRxiv https://doi.org/10.1101/2022.01.16.476530](https://doi.org/10.1101/2022.01.16.476530) (2022).
- Jones, D. L. & Rando, T. A. Emerging models and paradigms for stem cell ageing. *Nat. Cell Biol.* **13**, 506–512 (2011).
- Jasper, H. Intestinal stem cell ageing: origins and interventions. *Annu. Rev. Physiol.* **82**, 203–226 (2020).
- de Haan, G. & Lazare, S. S. Aging of hematopoietic stem cells. *Blood* **131**, 479–487 (2018).
- Reddy, P., Memczak, S. & Belmonte, J. C. I. Unlocking tissue regenerative potential by epigenetic reprogramming. *Cell Stem Cell* **28**, 5–7 (2021).
- Nevedomskaya, E. et al. CE-MS for metabolic profiling of volume-limited urine samples: application to accelerated aging TTD mice. *J. Proteome Res.* **9**, 4869–4874 (2010).
- Wang, X., Ge, J., Tredget, E. E. & Wu, Y. The mouse excisional wound splinting model, including applications for stem cell transplantation. *Nat. Protoc.* **8**, 302–309 (2013).
- Pau, G. & Reeder, J. HTSeqGenie: A NGS analysis pipeline. R package (v.4.2.1 and v.4.4.1) version <https://bioconductor.org/packages/release/bioc/html/HTSeqGenie.html> (2021).

35. Law, C. W., Chen, Y., Shi, W. & Smyth, G. K. voom: precision weights unlock linear model analysis tools for RNA-seq read counts. *Genome Biol.* **15**, R29 (2014).
36. Korotkevich, G., Sukhov, V. & Sergushichev, A. Fast gene set enrichment analysis. Preprint at *bioRxiv* <https://doi.org/10.1101/060012> (2021).
37. Matys, V. et al. TRANSFAC and its module TRANSCompel: transcriptional gene regulation in eukaryotes. *Nucleic Acids Res.* **34**, D108–D110 (2006).
38. Rouillard, A. D. et al. The harmonizome: a collection of processed datasets gathered to serve and mine knowledge about genes and proteins. *Database (Oxford)* **2016**, baw100 (2016).
39. Arneson, A. et al. A mammalian methylation array for profiling methylation levels at conserved sequences. *Nat. Commun.* **13**, 783 (2022).
40. Zhou, W., Triche, T. J.Jr., Laird, P. W. & Shen, H. SeSAMe: reducing artifactual detection of DNA methylation by Infinium BeadChips in genomic deletions. *Nucleic Acids Res.* **46**, e123 (2018).
41. Jauchico, A., Sangaraju, D. & Shahidi-Latham, S. K. A rapid derivatization based LC–MS/MS method for quantitation of short chain fatty acids in human plasma and urine. *Bioanalysis* **11**, 741–753 (2019).
42. Dunn, W. B. et al. Mass appeal: metabolite identification in mass spectrometry-focused untargeted metabolomics. *Metabolomics* **9**, 44–66 (2013).
43. Kind, T. et al. Identification of small molecules using accurate mass MS/MS search. *Mass Spectrom. Rev.* **37**, 513–532 (2018).

Acknowledgements

We thank M. Schwarz for administrative support. We also thank R. Russell for help with bioluminescence imaging in p16-luc mice. This study was supported by the Universidad Católica San Antonio de Murcia and Fundación Dr. Pedro Guillén. The cartoon images of mice and tissues were created with BioRender.com.

Author contributions

K.B., P.R., H.J. and J.C.I.B. designed all the experiments, prepared the figures and wrote the manuscript. P.R., M.Y., I.G.G., S.S., C.W., Y. Luque, K.S., T.H., C.R.E. and J.P. performed the *in vivo* experiments. K.B., L.S., M.P. and J.A.V.H. performed the bioinformatics analysis. Z.L., F.K.C. and D.S. performed the metabolomics analysis. Q.L., W.R.W., and W.S. performed the lipidomics analysis. Y. Liang contributed to NGS. C.R.E., E.N.D. and P.G.G. contributed to the analysis and reagents. A.H. and S.H. analyzed the DNA methylation data.

Competing interests

The authors declare no competing interests.

Additional information

Extended data are available for this paper at <https://doi.org/10.1038/s43587-022-00183-2>.

Supplementary information The online version contains supplementary material available at <https://doi.org/10.1038/s43587-022-00183-2>.

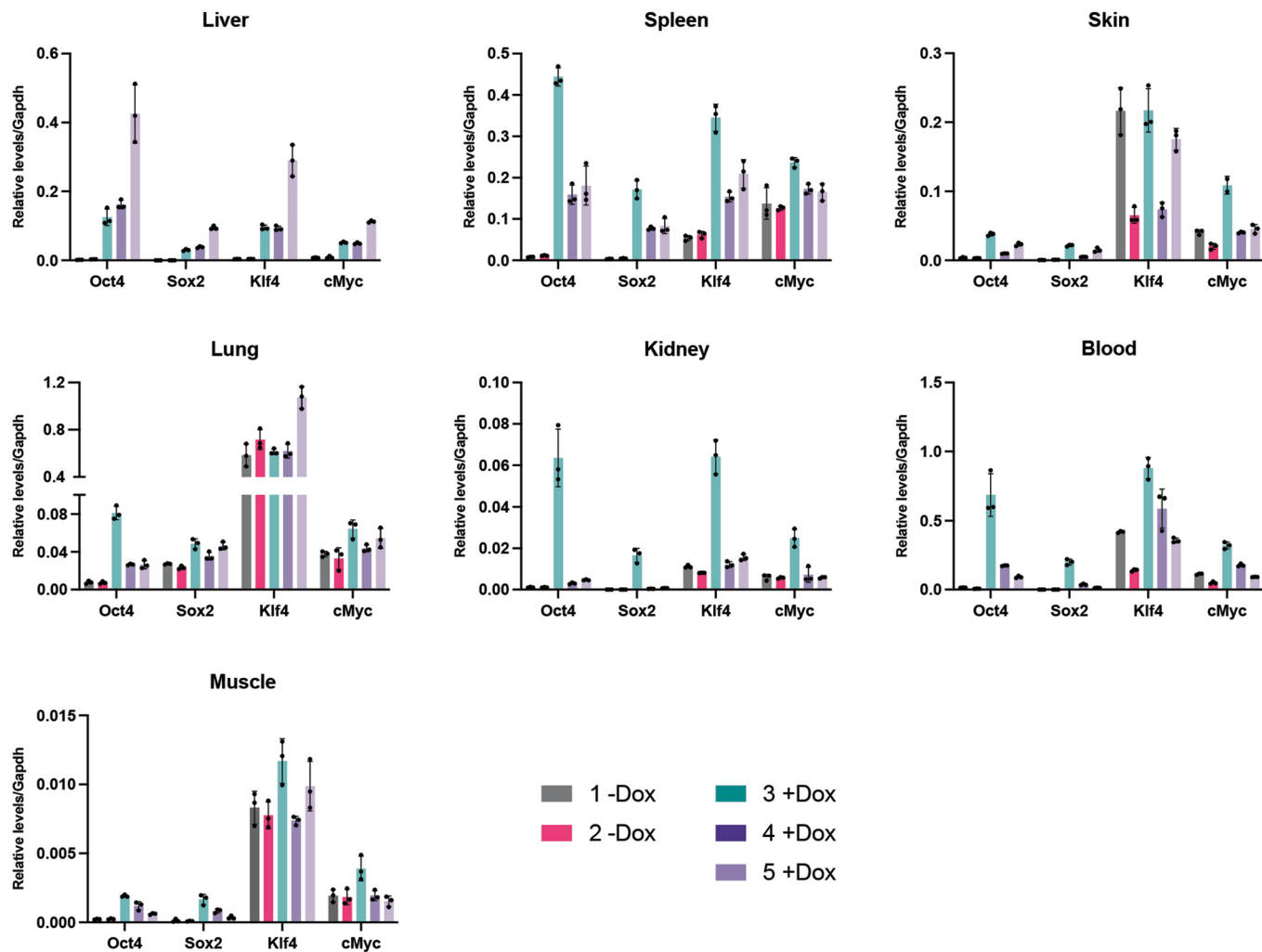
Correspondence and requests for materials should be addressed to Heinrich Jasper or Juan Carlos Izpisua Belmonte.

Peer review information *Nature Aging* thanks Jesus Avila, George Daley and the other, anonymous, reviewer(s) for their contribution to the peer review of this work.

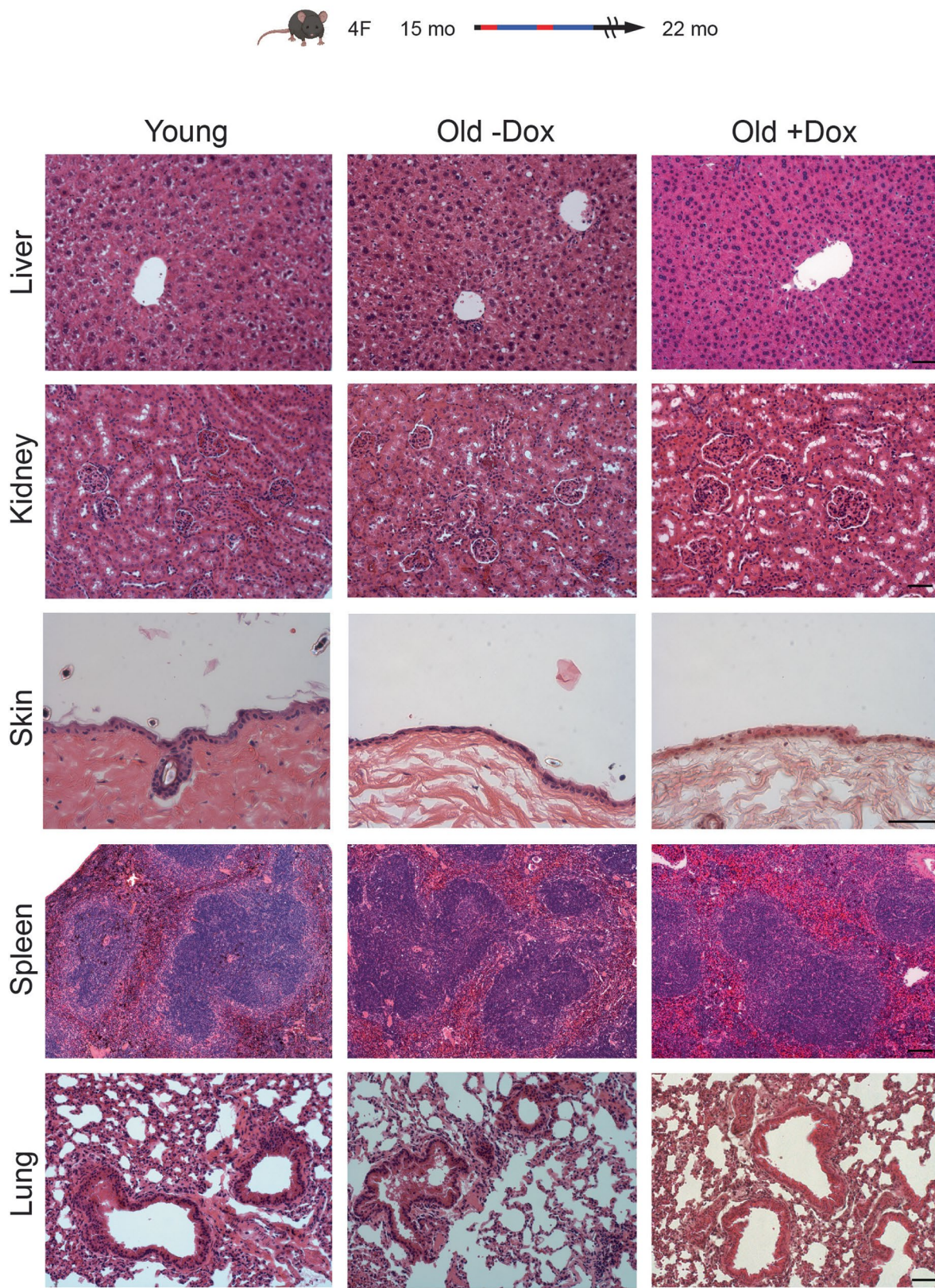
Reprints and permissions information is available at www.nature.com/reprints.

Publisher's note Springer Nature remains neutral with regard to jurisdictional claims in published maps and institutional affiliations.

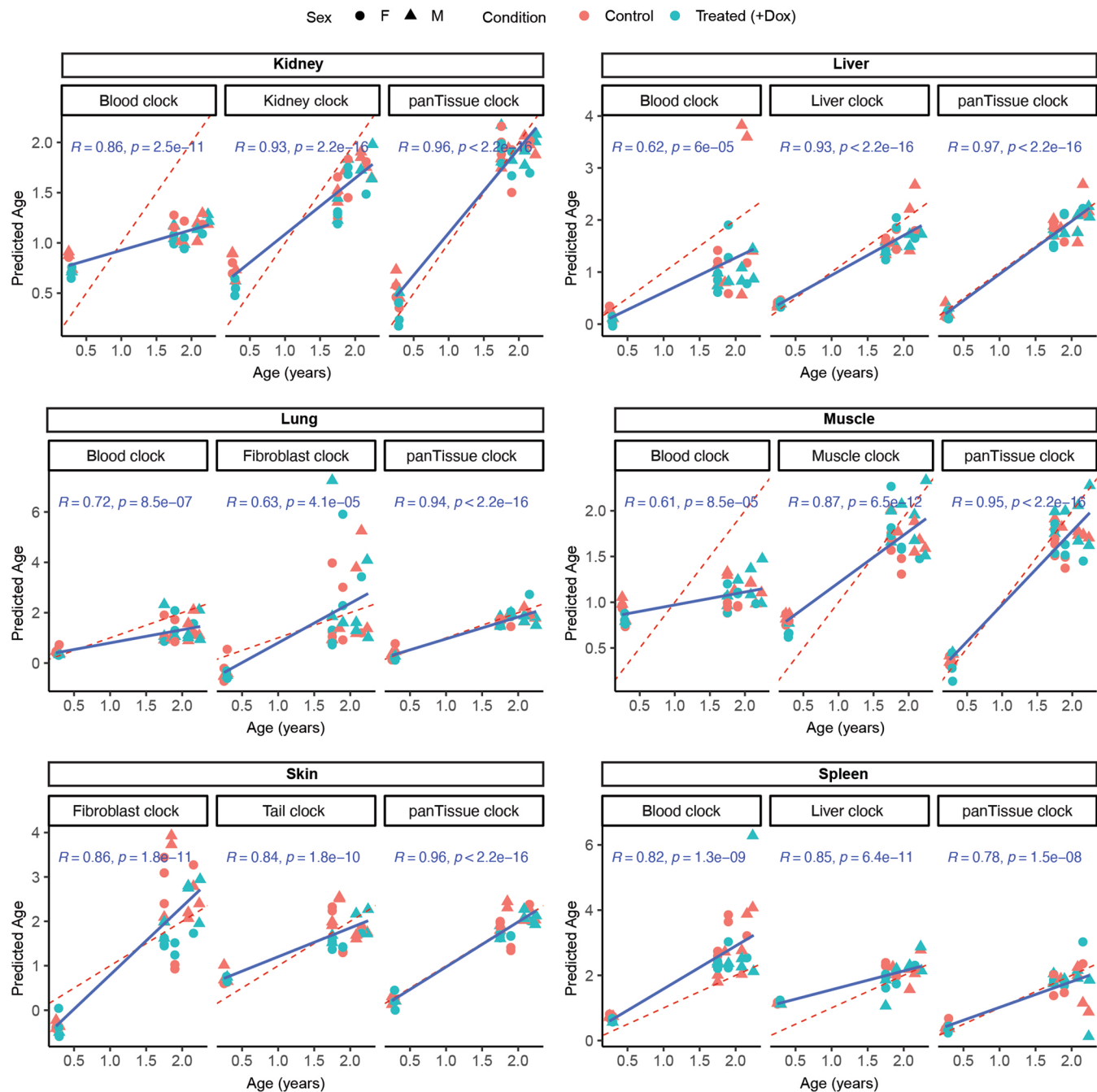
© The Author(s), under exclusive licence to Springer Nature America, Inc. 2022



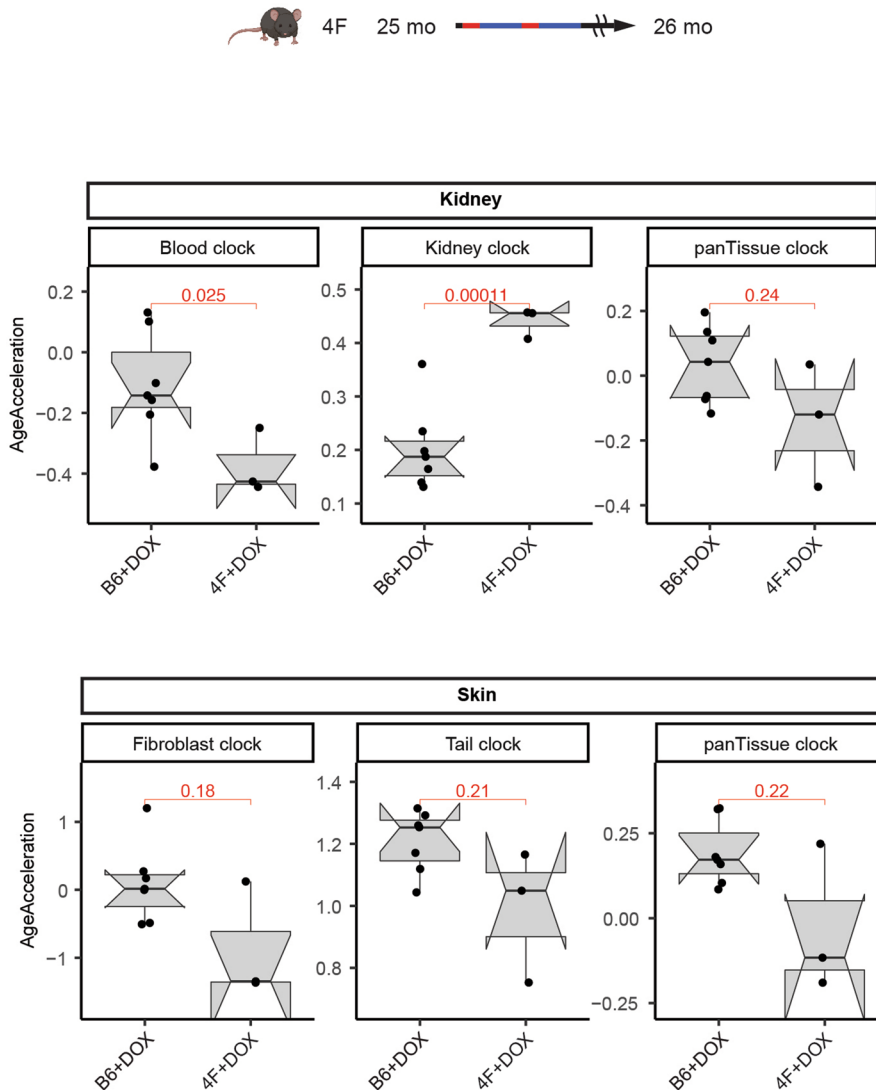
Extended Data Fig. 1 | Expression of reprogramming factors in tissues. The expression levels of reprogramming factors (Oct4, Sox2, Klf4 and cMyc) were measured in 9 months old 4F mice tissues after 48 hr of doxycycline treatment. $n=2$ (-Dox) and $n=3$ (+Dox) independent biological mice. The data are represented as mean \pm SD.



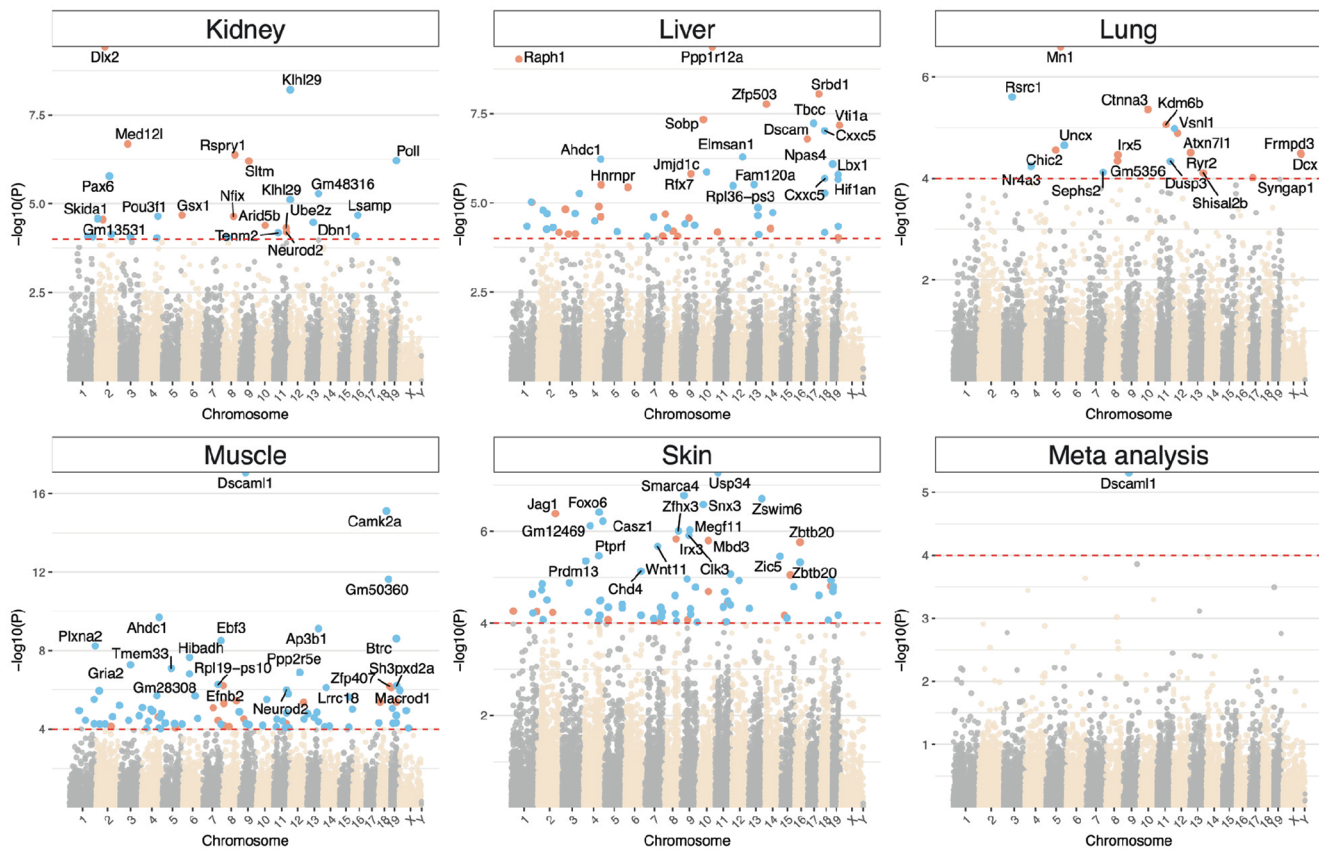
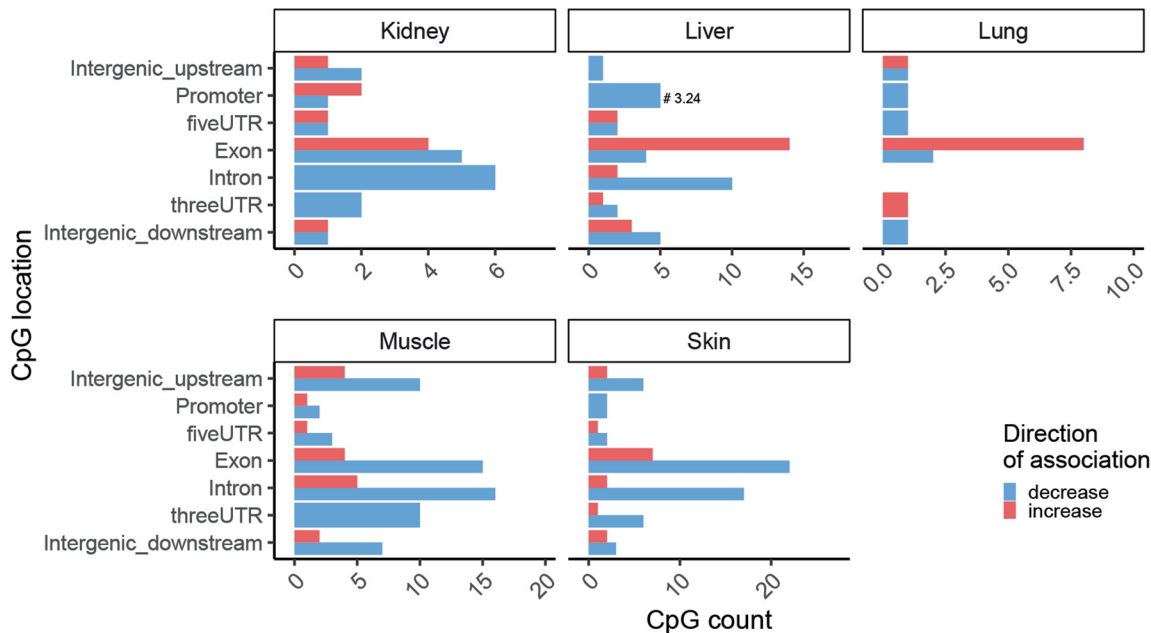
Extended Data Fig. 2 | Histological analysis of tissues. Representative images of the liver, kidney, skin, spleen and lung tissues from 7 months treated long-term partial reprogramming mice were collected at the end of the treatment. The tissues from the doxycycline treatment were compared to similar age untreated and young 4 F mice. Similar phenotypes were observed in 5 pairs of untreated and treated mice. Scale bar, 50 μ m (liver, kidney, skin and lung) and 100 μ m (spleen). Representative images are from $n=1$ mouse. Tissues were evaluated from $n=5$ (4 F -Dox) and $n=5$ (4 F + Dox) independent biological mice.



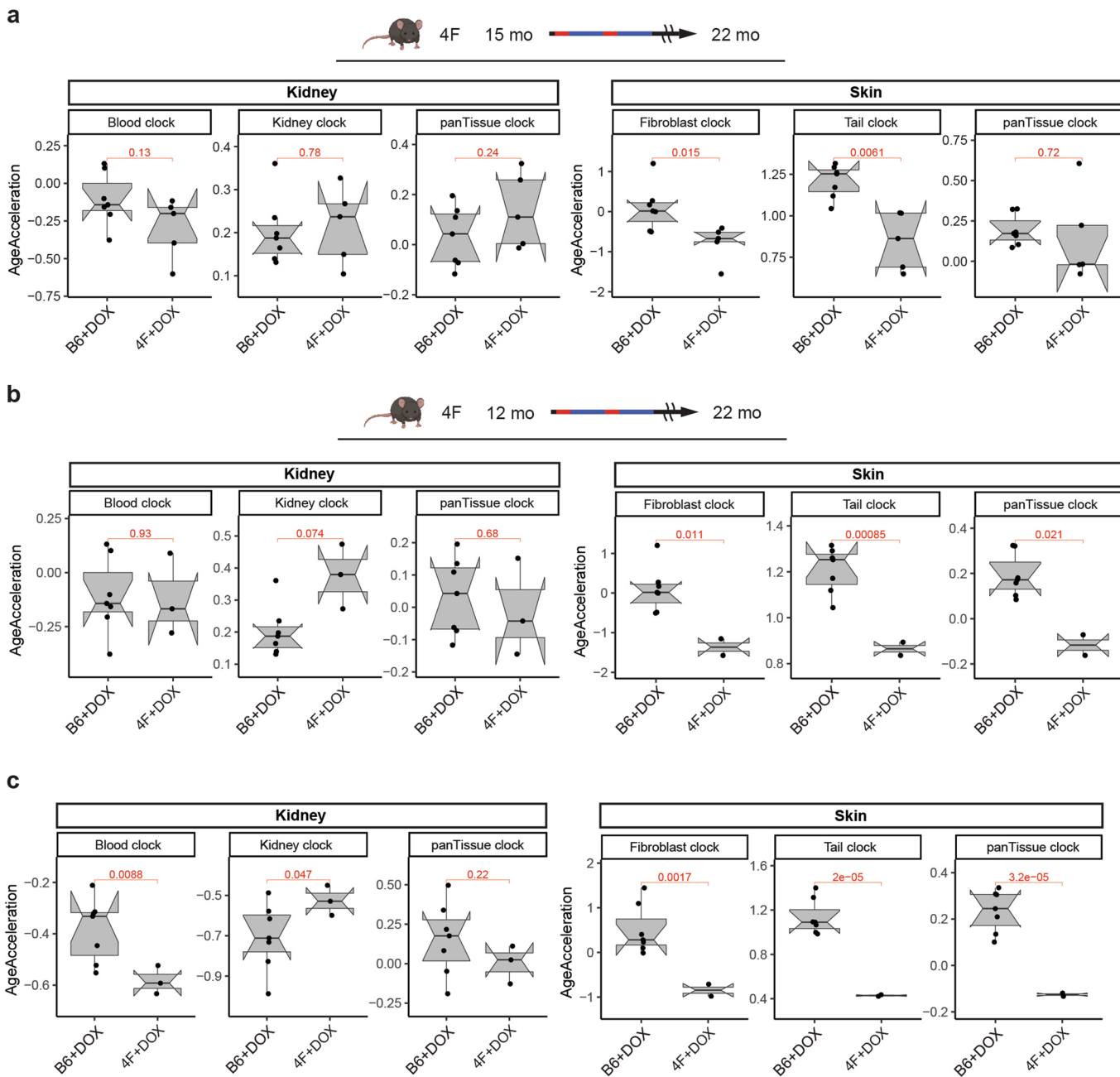
Extended Data Fig. 3 | Epigenetic clock analysis of tissues. Scatter plots of DNA methylation age (PredictedAge) (y-axis) versus chronological age (x-axis) of different tissues from 4F mice. DNAm age analysis is based on LUC clocks trained on either individual or pan-tissues. Kidney, Liver, Lung and Spleen: n=19 (Control) and n=17 (Treated). Muscle: n=18 (Control) and n=17 (Treated). Skin: n=20 (Control) and n=16 (Treated). Controls include 4F-Dox and B6 +Dox. Cor: Pearson correlation (cor); p: P-value from two-sided Student's t-test; Err: Mean absolute error.



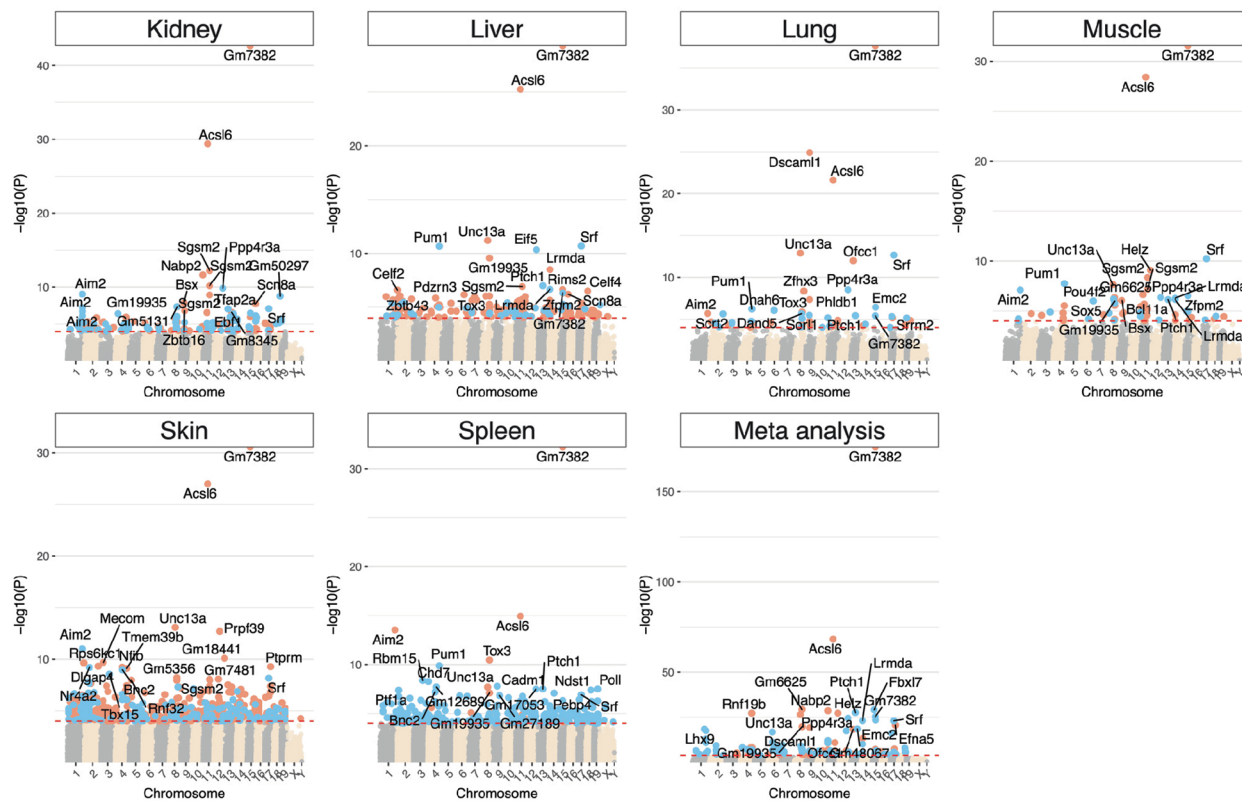
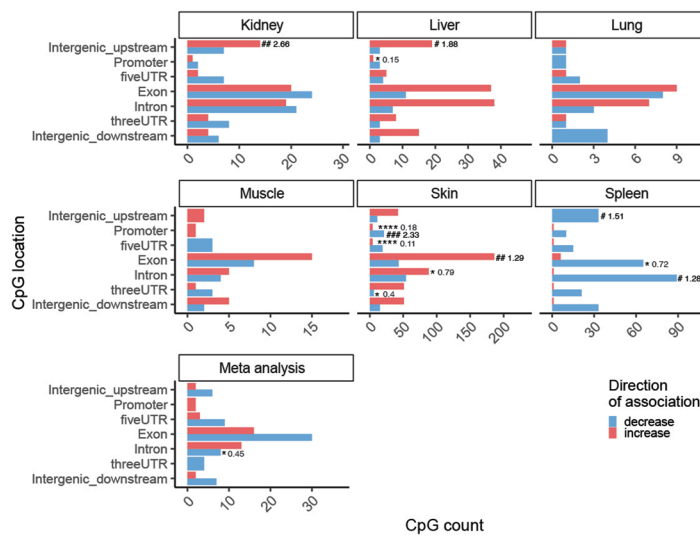
Extended Data Fig. 4 | Epigenetic clock analysis of tissues from short-term partial reprogrammed mice. Measurement of DNA methylation age of kidney and skin of 4F mice after short-term partial reprogramming using elastic net (EN) clocks trained on indicated tissues. n = 7 (B6 + doxycycline) and n = 3 (4F + doxycycline) independent biological mice. Age accelerations are the residuals of the predicted age regressed on the chronological age of each sample. The mean differences were examined by a two-sided Student t-test of age acceleration differences between the groups. The P values are reported in each panel. Boxes show the interquartile range of the age accelerations. The notches indicate the 95% confidence interval of the median. The whiskers represent 1.5*IQR length of the age accelerations.

**a****b**

Extended Data Fig. 5 | Distribution of CpG sites in tissues of short-term partial reprogrammed mice. **a**, Manhattan plots showing the distribution of hyper and hypomethylated CpGs in different tissues from 26 months old mice (4F -Dox $n=3$ and 4F +Dox $n=3$). The EWAS is done by linear regression model of the treatment vs the controls. The coordinates are estimated based on the alignment of Mammalian array probes to *mus musculus* mm10 genome. Top 15 CpGs was labeled by the neighboring genes. Red dashed line indicates $P < 10^{-4}$. **b**, Horizontal bars showing the CpG locations in the genome of tissues. The orange color denotes hypermethylated and blue color denotes hypomethylated CpGs in treated vs control animals. Fisher's Exact Test is used to examine the proportional change than the background; # two-sided P -value < 0.05 ; odd ratios are reported on the bars with significant proportional change.



Extended Data Fig. 6 | Epigenetic clock analysis of tissues from long-term partial reprogrammed mice. **a,b,** Measurement of DNA methylation age of kidney and skin of 4F mice after long-term partial reprogramming using elastic net (EN) clocks trained on indicated tissues. **a,** DNA methylation age acceleration in 4F mice after seven months of treatment starting at 15 months of age. $n=7$ (B6 + doxycycline) and $n=5$ (4F + doxycycline) independent biological mice. **b,** DNA methylation age acceleration in 4F mice after ten months of treatment starting at 12 months of age. $n=7$ (B6 + doxycycline) and $n=3$ (4F + doxycycline) independent biological mice. **c,** DNA methylation age acceleration of kidney and skin of 4F mice after ten months of treatment starting at 12 months of age using Lifespan Uber Correlation (LUC) clocks trained on indicated tissues. $n=7$ (B6 + doxycycline) and $n=3$ (4F + doxycycline) independent biological mice. Age accelerations are the residuals of the predicted age regressed on the chronological age of each sample. The mean differences were examined by a two-sided Student t-test of age acceleration differences between the groups. The P values are reported in each panel. Boxes show the interquartile range of the age accelerations. The notches indicate the 95% confidence interval of the median. The whiskers represent $1.5 \times \text{IQR}$ length of the age accelerations.

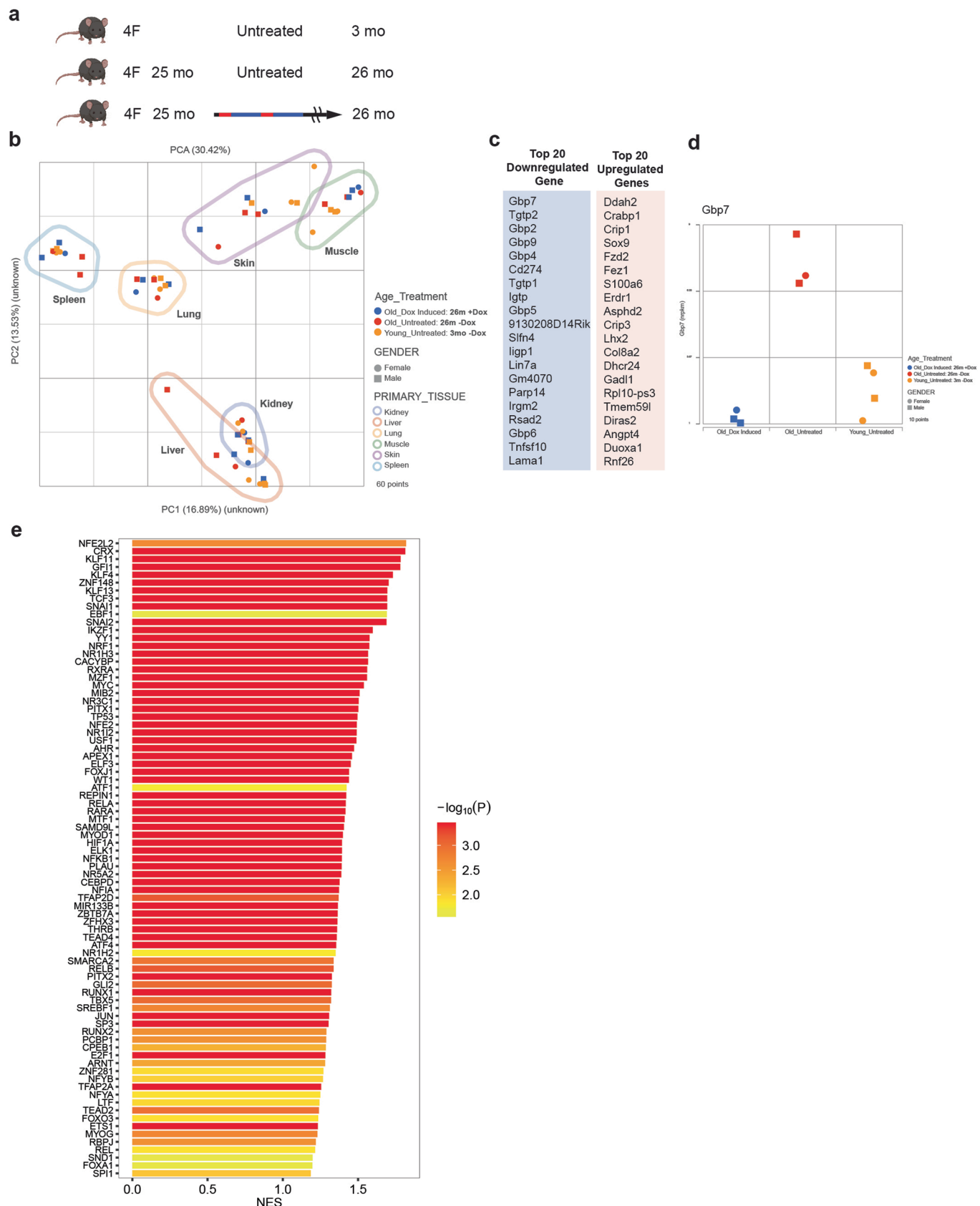
**a****b****c**

Top ■ hypermethylated:	
Symbol	GeneRegionalID
Gm7382	Gm7382_Promoter
Acsl6	Acsl6_Exon
Unc13a	Unc13a_Exon
* Prpf39	Prpf39_fiveUTR
* Mecom	Mecom_Intron
Rps6k1	Rps6k1_Intergenic_downstream
* Dlgap4	Dlgap4_threeUTR
* Ptprm	Ptprm_Exon
Nfib	Nfib_Exon
* Tmem39b	Tmem39b_threeUTR
Gm5356	Gm5356_Intergenic_downstream
Gm7481	Gm7481_Intergenic_downstream
* Sgsm2	Sgsm2_Exon
Rnf32	Rnf32_Intergenic_downstream
Gm6625	Gm6625_Intergenic_downstream
Supt6	Supt6_Exon
Gm18494	Gm18494_Intergenic_downstream
Sic35b3	Sic35b3_Intergenic_downstream

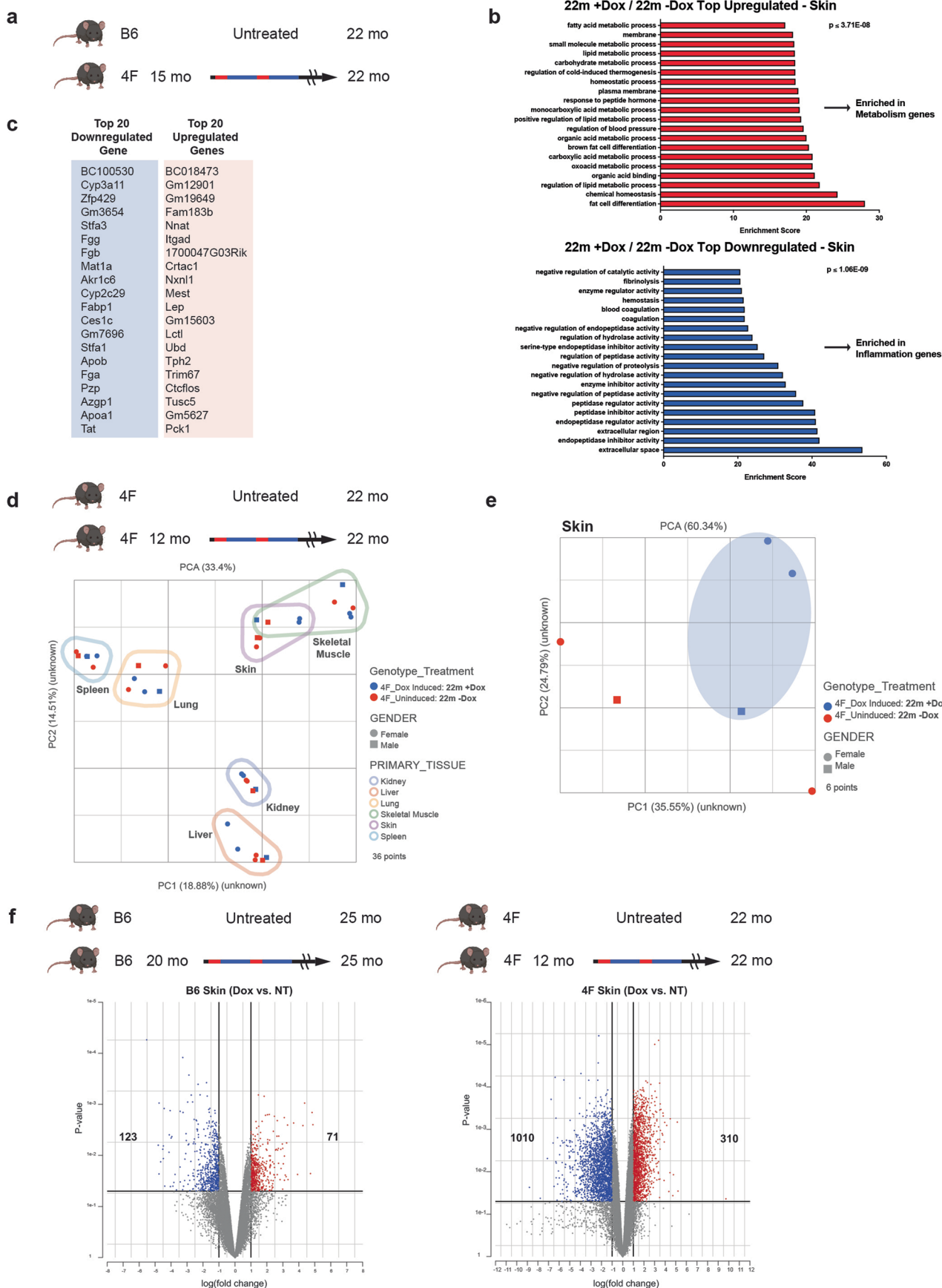
Top ■ hypomethylated:	
Symbol	GeneRegionalID
NA	NA
Aim2	Aim2_Intron
Nr4a2	Nr4a2_Intron
NA	NA
Bnc2	Bnc2_Intron
Tbx15	Tbx15_Intron
Srf	Srf_Exon
Zeb2	Zeb2_Intergenic_upstream
Nr4a2	Nr4a2_fiveUTR
Gm8730	Gm8730_Intergenic_upstream
Slc2a12	Slc2a12_fiveUTR
Lrmida	Lrmida_Intron
* Bdnf	Bdnf_fiveUTR
Zeb2	Zeb2_Intergenic_downstream
Irs1	Irs1_Exon
Bnc2	Bnc2_Intron
Aim2	Aim2_Intron

*Significant DE genes in skin.

Extended Data Fig. 7 | Distribution of CpG sites in tissues of long-term partial reprogrammed mice. **a**, Manhattan plots showing the distribution of hyper and hypomethylated CpGs in different tissues from 22 months old mice. $n=5$ (4 F + Dox) and $n=5$ (4 F - Dox) independent biological mice. The EWAS is done by linear regression model of the treatment vs the controls. The coordinates are estimated based on the alignment of Mammalian array probes to *mus musculus* mm10 genome. Top 15 CpGs was labeled by the neighboring genes. Red dashed line indicates $P < 10^{-4}$. **b**, Horizontal bars showing the CpG locations in the genome of tissues. The orange color denotes hypermethylated and blue color denotes hypomethylated CpGs in treated vs control animals. # indicates positive association and *indicates negative association. Fisher's Exact Test is used to examine the proportional change than the background; odd ratios are reported on the bars with significant proportional change. The P values (#, * <0.05 , **, ** <0.01 , ***, ***, *** <0.001 , **** <0.0001); the odd ratio values are reported on the bars. **c**, The list of top hyper and hypomethylated CpGs and the closest gene. The asterisk denotes the genes differentially expressed in skin.

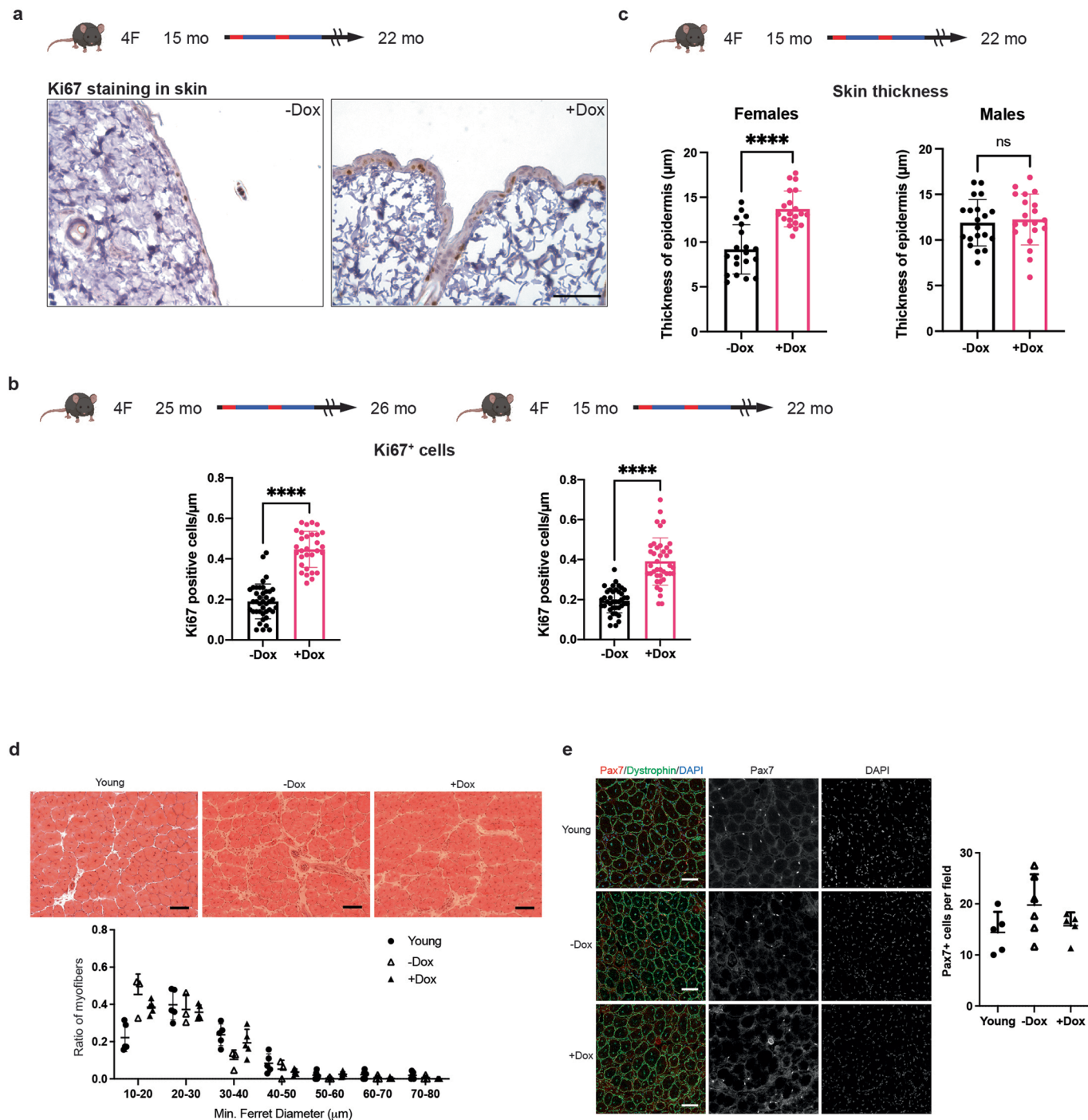


Extended Data Fig. 8 | Transcriptomic analysis of tissues of short-term partial reprogrammed mice. **a**, Transcriptional profiling of 25 months old 4F mice after 1 month of treatment by comparing to untreated and young 4F mice (3 mo). $n=4$ (old 4F -Dox), $n=3$ (old 4F +Dox) and $n=4$ (young 4F -Dox) independent biological mice. **b**, Plot of principal components (PC1 and PC2) obtained from the principal component analysis of tissues from untreated and treated male and female mice at 26 months of age and young 4F mice. **c**, The list of top 20 upregulated and downregulated genes. **d**, A dot plot showing the downregulation of Gbp7 gene expression in treated mice and comparable to young control. **e**, Transcription factor motif enrichment analysis in differentially expressed genes.



Extended Data Fig. 9 | See next page for caption.

Extended Data Fig. 9 | Transcriptional profiling of long-term treated 4F mice and doxycycline treated B6 mice. **a**, Transcriptional profiling of 22 months old 4F mice after 7 months of treatment by comparing to untreated B6 mice. $n=5$ (B6 -Dox) and $n=5$ (4F +Dox) independent biological mice. **b**, Gene ontology (GO) analysis of RNA-seq data of skin showing the top upregulated and downregulated genes. DEG list cutoffs defined as $P < 0.05$ and LFC of 2. **c**, List of top downregulated and upregulated genes in the skin. **d**, Plot of principal components (PC1 and PC2) of tissues from 10 months treated 4F mice analyzed at 22 months of age. $n=3$ (4F -Dox) and $n=3$ (4F +Dox) independent biological mice. **e**, Plot of principal components (PC1 and PC2) of the skin comparing control and treated mice. **f**, Volcano plots of RNA-seq data of skin generated by comparison of 5 months doxycycline treated B6 mice (control and treated) and 10 months treated 4F mice. For B6 +/-Dox controls, $n=2$ (B6 -Dox) and $n=2$ (B6 +Dox) independent biological mice. For 4F 10 month treated, $n=3$ (4F -Dox) and $n=3$ (4F +Dox) independent biological mice.



Extended Data Fig. 10 | Analysis of skin and skeletal muscle regeneration after long-term partial reprogramming. **a**, Representative images of immunostaining of Ki67 positive cells in the skin of 4F mice at 22 months after long-term partial reprogramming. Scale bar, 50 μm . **b**, Quantification of Ki67 positive cells in the skin of 4F mice after short-term and long-term partial reprogramming in 26 (-Dox $n=4$ and +Dox $n=3$) and 22 months (-Dox $n=4$ and +Dox $n=4$) 4F mice, respectively. 3 sections per mice were used for quantification. **c**, Epidermal thickness of skin in 4F mice at 22 months after long-term partial reprogramming. Females (-Dox $n=2$ and +Dox $n=2$) and Males (-Dox $n=2$ and +Dox $n=2$), 2 sections per mice were used for quantification. **d**, Representative histological images of TA muscle and quantification of muscle fiber size of Young (3-months) and 7-months treated (starting at 15 months of age until 22 months) 4F mice 10 days after cardiotoxin injection. Scale bar, 100 μm . **e**, Immunostaining of Pax7 and dystrophin and quantification of Pax7⁺ cells in TA muscle 10 days after cardiotoxin injection $n=5$ (Young), $n=6$ (-Dox) and $n=5$ (+Dox) independent biological mice. Scale bar, 50 μm . For all relevant figures, data are represented as mean \pm SD. **** $P < 0.0001$ values according to two-tailed Student's t-test.

Reporting Summary

Nature Portfolio wishes to improve the reproducibility of the work that we publish. This form provides structure for consistency and transparency in reporting. For further information on Nature Portfolio policies, see our [Editorial Policies](#) and the [Editorial Policy Checklist](#).

Statistics

For all statistical analyses, confirm that the following items are present in the figure legend, table legend, main text, or Methods section.

n/a Confirmed

- The exact sample size (n) for each experimental group/condition, given as a discrete number and unit of measurement
- A statement on whether measurements were taken from distinct samples or whether the same sample was measured repeatedly
- The statistical test(s) used AND whether they are one- or two-sided
Only common tests should be described solely by name; describe more complex techniques in the Methods section.
- A description of all covariates tested
- A description of any assumptions or corrections, such as tests of normality and adjustment for multiple comparisons
- A full description of the statistical parameters including central tendency (e.g. means) or other basic estimates (e.g. regression coefficient) AND variation (e.g. standard deviation) or associated estimates of uncertainty (e.g. confidence intervals)
- For null hypothesis testing, the test statistic (e.g. F , t , r) with confidence intervals, effect sizes, degrees of freedom and P value noted
Give P values as exact values whenever suitable.
- For Bayesian analysis, information on the choice of priors and Markov chain Monte Carlo settings
- For hierarchical and complex designs, identification of the appropriate level for tests and full reporting of outcomes
- Estimates of effect sizes (e.g. Cohen's d , Pearson's r), indicating how they were calculated

Our web collection on [statistics for biologists](#) contains articles on many of the points above.

Software and code

Policy information about [availability of computer code](#)

Data collection	Olympus IX51 microscope was used to histology images. ZEISS Zen software (v2.3 blue edition) was used to perform confocal imaging. Xcalibur Software version 4.2 is used for metabolomics data collection. Analyst 1.6.3 and Lipidlyzer platform were used to collect lipids data.
Data analysis	For image analysis NIH ImageJ (Fiji) software version 2.1.0/1.53c was used. For preparing plots and statistical analysis Prism version 8 (GraphPad Software) was used. Partek Flow Genomic Analysis Software version 2.3 and Enrichr (https://maayanlab.cloud/Enrichr/) were used for analysis of RNA-seq data. Compound Discoverer version 3.1, TraceFinder version 4.1, Polly platform version 1 (Elucidata Corporation) were used for metabolomics data processing. The SCIEX Lipidlyzer™ Platform, MultiQuant3.0.2, and Polly platform version 1 (Elucidata Corporation) were used for lipid data analysis

For manuscripts utilizing custom algorithms or software that are central to the research but not yet described in published literature, software must be made available to editors and reviewers. We strongly encourage code deposition in a community repository (e.g. GitHub). See the Nature Portfolio [guidelines for submitting code & software](#) for further information.

Data

Policy information about [availability of data](#)

All manuscripts must include a [data availability statement](#). This statement should provide the following information, where applicable:

- Accession codes, unique identifiers, or web links for publicly available datasets
- A description of any restrictions on data availability
- For clinical datasets or third party data, please ensure that the statement adheres to our [policy](#)

DNA methylation and RNA-seq data are deposited in the Gene Expression Omnibus under the accession number GSE190665 and SuperSeries accession number GSE190986. Metabolomics and lipidomics raw data can be found in supplementary tables 8 and 9 (4F mice serum) and 10 and 11 (B6 mice serum). The raw data for

the figures and other data supporting the findings in the study are available upon request from the corresponding author. MassBank of North America (MoNA, <https://mona.fiehnlab.ucdavis.edu/>), and commercial mzCloud (Thermo Fisher Scientific) mass spectral database were used.

Field-specific reporting

Please select the one below that is the best fit for your research. If you are not sure, read the appropriate sections before making your selection.

Life sciences Behavioural & social sciences Ecological, evolutionary & environmental sciences

For a reference copy of the document with all sections, see nature.com/documents/nr-reporting-summary-flat.pdf

Life sciences study design

All studies must disclose on these points even when the disclosure is negative.

Sample size	The samples sizes for each experiment are indicated in the figure legends. No statistical methods were used to predetermine sample size. Sample size was chosen based on the sample availability and statistic relevance. Sample size was at least n=3 independent biological replicates.
Data exclusions	No data were excluded.
Replication	Number of biological replicates are described in figure legends.
Randomization	No randomization method was used. Animals and samples were randomly allocated into experimental groups. Equal number of both the gender mice were included to minimize sex differences.
Blinding	No blinding was performed during in vivo experiment, tissue collections and statistical analysis. Blinding was done during analysis and quantification of histology data.

Reporting for specific materials, systems and methods

We require information from authors about some types of materials, experimental systems and methods used in many studies. Here, indicate whether each material, system or method listed is relevant to your study. If you are not sure if a list item applies to your research, read the appropriate section before selecting a response.

Materials & experimental systems		Methods	
n/a	Involved in the study	n/a	Involved in the study
<input type="checkbox"/>	<input checked="" type="checkbox"/> Antibodies	<input type="checkbox"/>	<input checked="" type="checkbox"/> ChIP-seq
<input checked="" type="checkbox"/>	<input type="checkbox"/> Eukaryotic cell lines	<input checked="" type="checkbox"/>	<input type="checkbox"/> Flow cytometry
<input checked="" type="checkbox"/>	<input type="checkbox"/> Palaeontology and archaeology	<input checked="" type="checkbox"/>	<input type="checkbox"/> MRI-based neuroimaging
<input type="checkbox"/>	<input checked="" type="checkbox"/> Animals and other organisms		
<input checked="" type="checkbox"/>	<input type="checkbox"/> Human research participants		
<input checked="" type="checkbox"/>	<input type="checkbox"/> Clinical data		
<input checked="" type="checkbox"/>	<input type="checkbox"/> Dual use research of concern		

Antibodies

Antibodies used	Rabbit Anti-Ki67 mAb, Cell Signaling, #9027 (1:200 dilution) Mouse Anti-Pax7 mAb, DSHB, #Pax7-C (1:200 dilution) Rabbit Anti-Dystrophin pAb, Abcam #ab15277 (1:500 dilution) Goat anti-Mouse IgG2b antibody conjugate Alexa Fluor 488, Invitrogen, #A21141 (1:500 dilution) Goat anti-Mouse IgG2b antibody conjugate Alexa Fluor 647, Invitrogen, #A21242 (1:500 dilution)
-----------------	--

Validation	Information from manufacturer website was used for selecting the antibody. Ki67 antibody was validated by using stomach and testes as positive control and primary antibody was excluded for negative control. Anti-Pax7 (DSHB, Pax7-c) has been cited in at least 97 references such as an immunostaining application in mouse muscle tissues:Lineage Tracing Reveals a Subset of Reserve Muscle Stem Cells Capable of Clonal Expansion under Stress. Cell stem cell 24.6 (2019Jun 6): 944-957.e5. Anti-Dystrophin pAb (Abcam #ab15277) and secondary antibodies have been verified in PMID: 28752107.
------------	---

Animals and other organisms

Policy information about [studies involving animals](#); [ARRIVE guidelines](#) recommended for reporting animal research

Laboratory animals	Mice carrying a single copy of OSKM polycistronic cassette and rtTA transactivator was used. C57BL/B6 were used in some
--------------------	---

Laboratory animals

experiments. All animals were in C57BL/6J background. Both males and female mice were used. Young mice were 3 months old. Aged mice were 12-26 months of age. The mice were housed in a temperature-controlled room (21-23 °C) at 40-60% humidity with 12 hr light and dark cycle between 06:00 and 18:00 and free access to water and food.

Wild animals

This study did not involve wild animals.

Field-collected samples

The study did not involve samples collected from the field.

Ethics oversight

All animal procedures were performed according to NIH guidelines and approved by the Committee on Animal Care at the Salk Institute.

Note that full information on the approval of the study protocol must also be provided in the manuscript.